An ocean-only framework for correcting future CMIP oceanic projections from their present-day biases

Matthieu Lengaigne[1], S Pang[2,3], Y Silvy[4], V Danielli[5], S Gopika[5,6], K Sadhvi[5,6], C Rousset[2], C Ethé[2], R Person[2], G Madec[2], N Barrier[5], O Maury[5], C Menkes[1], S Nicol[1], T Gorgues[1], A Melet[1], K Guihou[1], and J Vialard[2]

[1]Affiliation not available
[2]LOCEAN/IPSL, Sorbonne Universités (UPMC, Univ Paris
[3]CIC-FEMD/ILCEC, Key Laboratory of Meteorological Disaster of Ministry of Education (KLME), Nanjing University of Information Science and Technology
[4]Climate and Environmental Physics, University of Bern
[5]MARBEC, University of Montpellier, IFREMER
[6]CSIR-National Institute of Oceanography

July 05, 2024

An ocean-only framework for correcting future CMIP oceanic projections from their present-day biases

M. Lengaigne[1,*], S. Pang[2,3], Y. Silvy[4], V. Danielli[1], S. Gopika[1,5], K. Sadhvi[1,5], C. Rousset[2], C. Ethé[2], R. Person[2], G. Madec[2], N. Barrier[1], O. Maury[1], C. Menkes, S. Nicol, T. Gorgues, A. Melet, K. Guihou, J. Vialard[2]

[1] MARBEC, University of Montpellier, IFREMER, IRD, France

[2]LOCEAN/IPSL, Sorbonne Universités (UPMC, Univ Paris 06)-CNRS-IRD-MNHN, France

[3]CIC-FEMD/ILCEC, Key Laboratory of Meteorological Disaster of Ministry of Education (KLME), Nanjing University of Information Science and Technology, Nanjing, China

[4]Climate and Environmental Physics, University of Bern, Bern, Switzerland

[5] CSIR- National Institute of Oceanography, Goa, India

Submitted to Earth's future in XX May 2024

Corresponding Author

Matthieu Lengaigne

E-Mail: matthieu.lengaigne@ird.fr

Abstract

This paper proposes an ocean-only dynamical framework to mitigate the influence present-day biases of Earth System Models (ESMs) on future regional ocean physical and biogeochemical projections. Initially, a control experiment is conducted using fluxes derived from an atmospheric reanalysis, excluding climate change signals. Subsequently, a climate change simulation is performed by adding historical and future fluxes perturbations from a selected ESM to these background realistic fluxes. Since part of the ESM surface heat fluxes perturbation is a direct feedback to the sea surface temperature (SST) warming, these fluxes perturbations are split into SST-dependent and independent components. The climate change simulation is forced by the independent component, while the SST-dependent component is modeled online as an SST relaxation to the control experiment, accounting for Newtonian cooling and long-wave radiative feedback.

This approach demonstrates that ESMs present-day biases can heavily impact the reliability of regional physical and biogeochemical ocean projections. For instance, the strong cold-tongue bias simulated by the IPSL-CM6A-LR model causes greater warming and chlorophyll decrease in the western than in the eastern equatorial Pacific, while our bias-corrected simulation shows opposite projected patterns. Sensitivity experiments applying heat, freshwater and momentum fluxes perturbations separately further indicate that thermodynamical and dynamical processes equally contribute to this warming pattern, highlighting the strong role of the Bjerknes feedback. This cost-effective method can be applied to any ESMs oceanic component to produce more reliable regional oceanic projections and understand the mechanisms driving the projected patterns.

1. Introduction

Relevance of global warming for blue and green oceans. As a result of human activities, global-mean sea surface temperature has raised by approximately 0.8°C compared to pre-industrial levels. Earth System Models (ESMs) indicates that this warming will further increase over the course of the 21st century under all of the Representative Concentration Pathways (RCPs), leading to rising sea level, altered the hydrological cycle, changes in atmospheric and oceanic circulation, stronger tropical cyclones and heavier rainfall (Masson-Delmote et al. 2021). For the green ocean, this warming will enhance upper ocean stratification, limiting nutrients supply to the euphotic zone (Kwiatkowski et al., 2020). This generally leads to projected global reductions in phytoplankton and net primary production (Bopp et al., 2013; Kwiatkowski et al., 2020). This decline is consistently amplified in higher trophic levels, including zooplankton (Kwiatkowski et al., 2019) and fish (Lotze et al., 2019). Due to warming-induced reduction in O2 solubility, increased stratification and reduced ventilation, ESMs consistently project a global decline of dissolved oxygen (Bopp et al., 2013; Kwiatkowski et al., 2020). The uptake of carbon by the oceans also leads to ocean acidification, extensively impacts marine species including corals (Pandolfi et al. 2011).

Uncertainties in ESMs regional projections. The impacts of global warming will be felt most strongly at regional scales. However, considerable uncertainties exist in regional ESMs projections, particularly in tropical regions, limiting our ability to provide useful information for the planning and implementation of appropriate adaptation measures. Projected SST pattern indeed largely controls the tropical regional rainfall projections, through the "warmer-get-wetter" paradigm (Xie et al. 2010) and the climate sensitivity (Sherwood et al., 2020) through the pattern effect (Stevens et al., 2016). Phytoplankton forms the base of the marine food web and O_2 is crucial for marine ecosystems at low O_2, where marine animals are unable to sustain aerobic metabolism. When averaged, ESMs display an "El Niño-like" and "Indian Ocean Dipole-like" warming pattern in the tropical Pacific/Atlantic and Indian Ocean (Xie et al., 2010; see Fig. 1a). However, tropical SST patterns projections vary considerably across models, ranging for instance from El Niño–like, zonally uniform to La Niña–like patterns in the Pacific (Huang and Ying, 2015), leading to large uncertainties in projected rainfall patterns (Ma and Xie, 2013) and ENSO amplitude changes (Beobide-Arsuaga et al., 2021). Despite a consistent

decrease of surface chlorophyll along the entire equatorial Pacific and Atlantic, ESMs display a highly uncertain change phytoplankton and primary production in tropical and subtropical oceans (Fig. 1b), which largely control the very diverse magnitude of the chlorophyll decline across ESMs (Bopp et al. 2013; Kwiatkowski et al., 2017). Similarly, ESMs project a consistent O2 decline outside the tropical band but inconsistent changes in the tropics (Fig. 1c) and more specifically in the oxygen minimum zones (Cabré et al., 2015). These regional physical and biogeochemical projections are crucial as they form the basis of risk assessments for critical open ocean marine ecosystems and ecosystem services, such as fisheries (Bindoff et al., 2019). Understanding the drivers behind the diversity of these regional projections has thus attracted considerable attention in the past decade (e.g. Clement et al., 1996; Collins, 2005; Liu et al., 2005; Xie et al., 2010; Kwiatkowski et al., 2017; Tagliabue et al., 2021).

Impact of ESMs biases. The persistent present-day biases simulated by ESMs pose a long-standing challenge to the reliability of the projected oceanic patterns in the tropics (Li et al., 2016ab; Seager et al., 2019; Yang et al., 2022). Physical biases include a strong equatorial Pacific cold tongue bias extending too far into the western Pacific, a warmer eastern than western equatorial Atlantic opposite to observations (Richter et al., 2020); and too cold subtropical gyres (Fig. 1a). On the biogeochemical side, ESMs generally overestimate chlorophyll concentrations in all tropics and southern ocean (Fig. 2b), and overestimate O2 concentrations at depth in the central and western Pacific and in the Arabian Sea OMZ (Fig. 2c) These climatological biases are thought to significantly influence the regional ESMs projections (Li et al. 2016, Luo et al. 2018, Seager et al. 2019, Heede and Fedorov, 2021). Statistical "emergent constraint" approaches (Brient et al. 2019), relying on statistical relationship across a model ensemble between a measurable aspect of the present-day climate and projected future climate response to correct future changes, have been proposed to mitigate the influence of background biases on projected patterns (Huang and Ying, 2015; Li et al., 2016ab, Kwiatkowski et al., 2017). These studies indicate that the removal of ESMs biases could result in a more pronounced El Niño-like warming pattern (Huang and Ying, 2015; Li et al., 2016a), a reduction of the IOD-like warming pattern (Li et al., 2016b). It also allowed to better constrain the tropical marine primary decline (Kwiatkowski et al., 2017), O2 changes in Southeastern Pacific OMZ (Almendra et al., 2024) or the ocean carbon sink (Terharr et al., 2022). However, some emergent constraints may be spurious, as they may be influenced by common structural model assumptions, rather than from an intrinsic underlying process, or by the use of subjective model metrics or spurious correlations unsupported by a plausible

mechanism (Knutti et al., 2017; Eyring et al., 2019; Sanderson et al., 2021), ultimately leading to biased and overconfident constrained projections. The primary objective of this paper is to propose an alternative dynamical framework to evaluate the influence of CMIP model biases on future oceanic projections.

Our approach: present-day bias correction. The objective of this study is to build an ocean-only modeling framework to assess the impact of model biases on projected ocean physical and biogeochemical responses and investigate their underlying mechanisms. To achieve this, we will incorporate external climate change forcing perturbations from ESMs into surface fluxes derived from an ocean model driven by detrended atmospheric reanalysis-derived forcing, ensuring that the background oceanic state closely aligns with observations. This approach significantly reduces present-day ESMs biases, enabling an assessment of these biases on future oceanic projections. This approach is the oceanic counterpart of dynamical atmospheric approaches developed to mitigate the influence of background atmospheric biases on future atmospheric projections. In these approaches, large-scale climate change changes from ESMs are imposed on a control atmospheric climate simulation forced with observed SST by modifying the boundary conditions of the regional (e.g. Adachi and Tomita 2020) or global (the amip-Future4K simulations from the CMIP6 protocol; see Webb et al. 2017) atmospheric models. This for more reliable atmospheric projections by correcting the ESM biases in boundary conditions.

Our approach: Accounting for air-sea flux SST dependency. However, since a portion of anomalous surface heat fluxes induced by climate change represent direct feedback to climate change-induced SST warming, it becomes necessary to separate the ESMs surface fluxes component that directly depends SST from the component that does not. The latter portion is used as a forcing flux input to the ocean model, while the former is modelled online as a relaxation of the SST from debiased historical and future simulations to the SST of the de-biased control simulation. This SST feedback coefficient, derived from ESMs surface variables, encompasses the Newtonian cooling negative feedback associated with latent heat fluxes via the Clausius-Clapeyron relationship, the negative feedback associated with upward long-wave radiation according to Stefan's law (Zhang and Li, 2014), and the positive downward longwave radiation feedback related to increasing temperature (Shakespeare and Roderick, 2022).

Our approach: Process-oriented studies. This modelling strategy can also help understanding the dominant processes shaping the physical and biogeochemical oceanic response to climate change. Varied processes have been proposed to explain the projected tropical response to climate change pattern. In the tropical Pacific, models projecting an El Niño-like warming pattern typically emphasize thermodynamical processes, such as a greater evaporative cooling at the equator than off-equator and in the western Pacific than in the eastern Pacific (Zhang and Li, 2014). Conversely, models that project a La Niña-like warming pattern typically emphasize ocean dynamical processes, notably the ocean dynamical thermostat mechanism (Clement et al., 1996). This mechanism impedes the warming in the central-eastern equatorial Pacific through a time delay in the response to warming between the surface and subsurface ocean, resulting in intensified ocean stratification (Clement et al., 1996; DiNezio et al., 2009). Additionally, the Bjerknes feedback (Bjerknes, 1969) can amplify equatorial changes in SST patterns through the coupling between the zonal SST gradient, the equatorial trade winds and the zonal thermocline slope (Held and Soden, 2006; Vecchi and Soden, 2007; Bayr et al., 2014). On biogeochemical side, increased stratification has been proposed as the leading hypothesis explaining the decline in primary production by reducing the nutrients supply to the euphotic zone (Bopp et al. 2013; Fu et al. 2016; Kwiatkowski et al., 2017). While this hypothesis may hold in oligotrophic regions, it may not apply in productive regions like upwellings, where ocean dynamics partly controls the productivity through its influence on the nutricline depth (Kwiatkowski et al., 2017). Similarly, the processes responsible for oxygen changes, which result from both physical (solubility, ventilation) and biological (respiration) processes are not well understood yet (Cabré et al. 2015; Oschlies et al. 2018). Our ocean-only framework allows for sensitivity experiments where heat, freshwater and momentum fluxes perturbations are applied separately. These simulations can then be used to delineate the relative role of thermodynamical and dynamical processes on the projected patterns.

Paper structure. The objective of the proposed modelling framework is to assess the influence of the mean-state ESMs biases on future projected physical and biogeochemical patterns and to identify the mechanisms driving these patterns. To achieve this, we propose a novel approach based on ocean-only simulations, where the background state more closely resemble observations compared to most ESMs. This approach involves introducing "externally forced" perturbations in surface heat, freshwater and wind stress fluxes derived from a given ESM, in addition to the background fluxes. These ocean-only simulations use the ocean component of the parent ESM, but with the ocean being forced by prescribed fluxes at

its boundaries instead of being coupled to an atmosphere. This methodology is illustrated with perturbations derived from two ESMs (IPSL-CM6A-LR and CNRM-ESM2-1) sharing the same oceanic component (NEMOv3.6), although the approach can be applied to any other ESMs. Section 2 describes the methodology employed to produce the spin-up and control simulations while Section 3 describes the methodology for deriving the climate change simulations. Section 4 demonstrates the robustness of the proposed methodology, illustrating the large impact of the IPSL-CM6A-LR and CNRM-ESM2-1 biases on the physical and biogeochemical projected changes for the tropical Pacific and discussing the mechanisms driving these projected changes. Section 5 provides a brief summary, discusses the present results in the context of the previous literature and lay out some perspectives of this work.

2. Methodology for spin-up and control simulations

2.1. The ocean model configuration

In the following, we illustrate this modelling framework in the context of the simulated climate by the IPSL-CM6A-LR (Boucher et al., 2020) and CNRM-ESM2-1 (Séférian et al. 2019) coupled models. These models share the same ocean model configuration NEMO3.6 (Madec et al. 2017), with a nominal horizontal resolution of 1◦ refined to 1/3◦ at the Equator, comprising 75 vertical levels (1 m at the surface to 200 m at the deepest levels). The physical component (OPA) of is coupled to the LIM3 sea-ice model (Rousset et al., 2015) and to the PISCES-v2 biogeochemical model (Aumont et al., 2015). Additionally, the ocean physical and biogeochemical components are employed in stand-alone mode, without the inclusion of the sea ice component, using the same configuration as in the coupled model. It is acknowledged that this configuration may result in localized temperature values falling below the freezing point in polar regions. To address this, the ocean temperature is capped to the freezing point in both the equation of state and in the calculation of the Brunt–Väisälä frequency, as proposed by Silvy et al. (2022).

2.2. Detrended atmospheric forcing

Detrended forcing. This section describes the ocean-only spin-up experiment, designed to simulate a stable oceanic mean state representative of the mid-20th century without climate change signals but with a natural variability comparable to that observed. The initial step is to

perform a long spin-up simulation, which is forced with bulk formulae using atmospheric inputs derived from the JRA-55 atmospheric reanalysis (Kobayashi et al. 2015) over the 1958 to 2022 period. Given that the climate change signal will be derived from the coupled model, it is important to ensure that the spin-up and control simulations exclude anthropogenically-driven signals. Some near-surface atmospheric parameters used as inputs for the bulk formulae indeed exhibit a clear upward trend over the historical period (Fig. 2a-c). This trend is exemplified by the 10-m air temperature and surface specific humidity, showing consistent increase, particularly pronounced over the tropical Indo-Pacific warm-pool region. Conversely, other variables like winds display a more varied signal, potentially unrelated to climate change. To ensure consistency, a point-wise linear detrending is applied to all the JRA-55 input parameters. The resulting globally-averaged evolution of JRA55 inputs is illustrated on Figure 2def. This straightforward linear detrending efficiently mitigates the long-term warming and moistening of the surface layers, while keeping interannual to multidecadal signals unaltered. Although alternative trend estimation methods, such as fitting a point-wise fourth-order polynomial to JRA55 entry variables, has been explored, they yielded similar results (not shown).

2.3. Bulk forced spin-up simulation

Bulk-forced spin-up and control simulation. The spin-up and control simulations strategy is schematized in Figure 3. The detrended near-surface atmospheric parameters described above are used as forcing for the spin-up simulation through bulk formulae. This simulation is initialized from the WOA at rest As illustrated in Figure 4a, the SST and other near-surface physical ocean parameters swiftly stabilize. Conversely, biogeochemical variables display notable drifts until the end of the first 65 years (Fig. 4bc). To achieve equilibrium in the solution of biogeochemical variables (and physical variables at depth), the last time step of this 65-year simulation is used as a restart to run another 65-year simulation using the same atmospheric forcing. This process is repeated six times to achieve a 455 years long spin-up simulation. The globally averaged chlorophyll signal stabilizes by the 4^{th} cycle, while the drift of the globally averaged oxygen signal at depth decreases considerably over time, although showing a modest positive trend until the end of the simulation. A similar evaluation, focusing on the eastern equatorial Pacific (Niño3 region; 140°E-90°E; 5°N-5°S), indicates a more rapid equilibration of the biogeochemical variables (Figure 4def). From the 3^{rd} cycle onwards, the Chl and O_2 concentration stabilize.

2.4. Flux-forced control simulation

Flux-forced CTL simulation. The objective of the control (CTL) experiment is to establish a baseline oceanic state devoid of climate change signals but encompassing realistic natural climate variability against which climate change simulations can be compared to. To apply our heat flux climate change simulation strategy, surface boundary conditions have to be applied as fluxes, not computed through bulk formulae. All necessary fluxes (heat, freshwater, salt, wind stress) from the last three cycles of the above bulk-forced spin-up simulation and required to force the control simulation are outputs of the bulk-forced simulation at a frequency of 3 hours, allowing to resolve the diurnal cycle and to remain close to bulk-forced simulation. A comprehensive description of all the flux components required to force the CTL simulation is provided in Silvy et al. (2022). A flux-forced simulation is simply driven by the fluxes derived from the bulk-forced simulation over the last three cycles, with initial conditions taken as the last time step of the fourth cycle of the bulk-forced experiment (Figure 3). The first cycle allows the ocean to adjust to the flux-forced framework, while the final two cycles constitute our CTL simulation against which all climate change simulations will be compared (Figure 3). Given that the fluxes originate from beneath sea-ice and are imposed onto the ocean, the sea ice model component is excluded from this oceanic configuration. As illustrated in Figure 4 the CTL SST, Chl and O_2 evolution closely follows that of the bulk-forced simulation for both the globally averaged and regional timeseries.

2.5. Reference simulation

Reference simulation. To validate our modelling framework to observations over the historical period, we also conducted a bulk-forced reference simulation (REF) using the original JRA55 atmospheric parameters prior to detrending. This simulation starts at the end of the fifth cycle of the spin-up simulation (Figure 3). As illustrated in Figure 4 it depicts an anthropogenically induced global warming trend, a global Chl decline and a global O_2 increase. However, these changes are rather heterogeneous, as shown in Figure 3def for the case of the eastern Pacific. Here, the warming trend is weaker and masked by the strong ENSO-related interannual variability, with O_2 concentrations decreasing while Chl remains relatively stable.

Forced vs. coupled climatological biases Figure 5 shows an evaluation of the biases in our REF simulation (left panels) compared to those of the IPSL-CM6A-LR coupled historical simulations (right panels) for SST and Chl and O_2. As anticipated, the climatological SST biases in the forced experiment are considerably weaker compared to those simulated in the coupled historical experiment (Fig. 5ab). For example, the cold tongue bias of up to -2°C across the equatorial Pacific in the coupled simulation, is considerably reduce in the REF simulation. Additionally, cold biases in the subtropical gyres and warm biases along the west coast of North America and in the Southern Ocean in the coupled simulation are corrected in REF simulation. However, our forced framework does not correct for the strong cold bias in the northwestern Atlantic. Tropical O_2 biases are also reduced in the forced simulation compared to the coupled one (Fig. 5ef). The coupled simulation strongly overestimate O2 concentrations in the Eastern Pacific and Arabian Sea OMZs, with biases ranging from +40 to /100 mmol.L^{-1} in regions where climatological O_2 concentrations are lower than 20 mmol.L^{-1}. This issue is mitigated in the REF simulation, where biases range between -20 and 20 mmol.L^{-1} in OMZ regions. The overestimated O_2 concentrations in the northern Indian Ocean and in the northeastern Pacific are also considerably reduced. However, REF simulation cannot correct for the overestimated O_2 concentrations in the central tropical Pacific and underestimates O_2 concentrations in the North Pacific subtropical gyre. Compared to SST and O_2, surface Chl biases are relatively similar in the forced and coupled simulations (Fig. 5cd). This might be due stem from the relatively weak Chl biases in the IPSL-CM6A-LR historical experiments (Fig. 5d) compared to those from most other ESMs (Fig. 1c).

3. Methodology for climate change simulations

3.1. Diagnosing future air-sea flux changes from ESMs

Scenarios. For the purpose of the CMIP6 exercise, after a long spin-up, multiple experiments were already conducted with the IPSL-CM6A-LR and CNRM-ESM2-1 coupled models.The IPSL-CM6A-LR model provides 32 members for the historical period (1850–2014) and 7 members for the SSP585 (Shared Socioeconomic Pathway 3-8.5; Gidden et al., 2019) scenario while the CNRM-ESM2-1 model provides 15 members for the historical period and 5 members for the SSP585 scenario.

CMIP preprocessing. The climate change (CC) simulations receive the same flux forcings as the CTL experiment, with additional perturbation corresponding to surface fluxes (heat, freshwater, wind-stresses) future changes. These perturbations are derived from the monthly-mean fluxes of a selected CGCM and are averaged across ensemble simulations covering both the historical and future period. Future changes (noted Δ) in air sea fluxes (noted F) are obtained as:

$$\Delta F(i,j,t) = F(i,j,t) - \overline{F(i,j,t)}$$

where the overbar denotes a temporal mean over the 1948-1967 period, and $F(i,j,t) = \langle F(i,j,\widetilde{t,k})\rangle_{k=1,2,..,n}$ is the ensemble mean flux over all available members k for the ESM ensemble considered. Ensemble averaging removes a substantial portion of the internal variability, yielding a reasonable approximation of external forcing. To mitigate residual natural noise resulting from the limited number of members in some scenario, a 25-year running mean smoothing is applied to the ensemble mean, denoted by $\widetilde{\square}$ in the above formula. In our approach, the internal variability (e.g. ENSO) in our CTL experiment corresponds to that in the detrended JRA55 dataset, repeated twice. In the climate change simulations, we apply the same internal variability, adding the low-frequency surface flux perturbations on top. Subtracting the two therefore extracts the externally-forced response, including the potential rectification of internal variability by changes in the mean state.

3.2. Heat flux changes: computing the SST-dependent "feedback" component

General approach. Previous studies have demonstrated that a significant portion of the air-sea heat flux response to climate change is strongly dependent on SST (e.g. Xie et al., 2010; Zhang and Li, 2014). While greenhouse gases only alter the surface radiative forcing by a few $W.m^{-2}$, the resulting SST warming can modify surface fluxes by a much larger magnitude, often several tenth of $W.m^{-2}$ (Pendergrass et al., 2018; Shakespeare and Roderick, 2022). For instance, a significant proportion of the increase in downward longwave flux is a direct feedback to the surface ocean warming, as a consequence of increased air temperature and moisture content, which in turn amplifies downward surface longwave fluxes. If our correction strategy significantly modifies SST projections, the resulting changes in air-sea fluxes must be accounted for to maintain physical coherence. This can be achieved by separating surface heat flux changes into a SST-dependent and SST-independent part as detailed in Zhang and Li

(2014) for latent heat fluxes and upward longwave radiation and Shakespeare and Roderick (2022) for downward longwave radiations. These derivations are synthetized below.

Latent feedback. While the weakening of the tropical circulation generally acts to warm the ocean, this warming directly increases latent heat fluxes via the Clausius-Clapeyron relationship, therefore acting as a negative feedback. Zhang and Li (2014) proposed a simple analytical development to derive the feedback coefficient related to latent heat fluxes. The bulk formula for surface latent heat flux can be expressed as:

$$Q_{LH} = \rho L C_E V\ (1 - RH e^{-\alpha \delta T}) q_s$$

where is ρ air density near the surface; C_E is the heat exchange coefficient of LH, , V is the surface wind speed, RH is relative humidity, and δT is the difference between SST and surface air temperature. Using Clausius Clapeyron relationship, and assuming that δT remains constant in the future, the change of Q_{LH} with respect to change in SST can be rewritten as:

$$\Delta Q_{LH}^{Fbk} = \lambda_{LH} \Delta \mathrm{SST}$$

where ΔQ_{LH}^{Fbk} denotes the part of future latent heat flux changes du to SST change (the "feedback" component) and $\lambda_{LH} = \frac{\overline{Q_{LH}}\, L_v}{R\, \overline{SST^2}}$, with L_v being the latent heat of condensation, R the ideal gas constant for water vapor and $\overline{Q_{LH}}$ the present-day climatological latent heat flux. $\Delta Q_{LH}^{For} = \Delta Q_{LH}^{\square} - \Delta Q_{LH}^{Fbk}$ denotes the "forcing" part of surface latent heat flux changes, i.e. the SST-independent part, related to changes in atmospheric wind speed, relative humidity, and air–sea temperature difference.

Longwave upward feedback. According to Stephan's law, upward longwave radiation primarily depends on the SST, constituting a negative feedback to the SST response rather than a direct radiative forcing resulting from increased CO_2 concentrations. Indeed, the change of upward longwave radiation at the ocean surface may be approximately written as :

$$\Delta Q_{LWU_{\square}}^{Fbk} = \lambda_{LWU_{\square}} \Delta SST$$

Where $\lambda_{LWU_{\square}} = 4\sigma \overline{SST^3}$, with σ being the ocean surface emissivity assumed to be unit. In that case, $\Delta Q_{LWU_{\square}}^{For}$ is negligible (not shown).

Longwave downward feedback. ESMs simulate an increase in downwelling longwave surface radiation, leading to warming of the upper ocean. In their analytical development, Zhang and Li (2014) considered $\Delta Q_{LWD_{\square}}$ as a forcing term, with no SST feedback component.

Nevertheless, the forcing component of the downward longwave radiation flux perturbations ($\Delta Q^{For}_{LWD_{\square}}$) due to the direct surface effect of greenhouse gases increase constitutes a relatively very small fraction (5-10%) of $\Delta Q_{LWD_{\square}}$ (Pendergrass et al., 2018; Shakespeare and Roderick, 2022). Most of $\Delta Q_{LWD_{\square}}$ warming effect results from a positive feedback ($\Delta Q^{Fbk}_{LWD_{\square}}$) to the ΔSST warming, through increased air temperature and moisture content, which in turn amplifies downward surface longwave fluxes. In a recent publication, Shakespeare and Roderick (2022) presented an explicit analytic expression for the radiative forcing and feedbacks, which capture more than 90% of $\Delta Q_{LWD_{\square}}$ in ESMs, with a typical error of less than 5%. Furthermore, the authors demonstrate that $\Delta Q^{Fbk}_{LWD_{\square}}$ can be decomposed into contributions from changes in temperature, specific humidity, water vapor height scale, and cloud fraction. They show that changes in temperature, specific humidity and height scale are closely linked to ΔSST and therefore that 90% of the $\Delta Q_{LWD_{\square}}$ increase can be attributed to a feedback from increasing ΔSST. Following their analytical development, $\Delta Q^{Fbk}_{LWD_{\square}}$ can be written as:

$$\Delta Q^{Fbk}_{LWD_{\square}} = \lambda_{LWD_{\square}} \Delta SST$$

Where $\lambda_{LWD_{\square}}$ gather the feedback contributions from temperature changes in the atmospheric column, changes in specific humidity and changes in water vapor scale related to temperature changes and can be directly expressed as a function of basic climatological surface variables available in the ESMs (for details refer to Shakespeare and Roderick (2022)).The part of longwave downward heat flux change due directly to the change of CO_2 and cloud cover change, which cannot directly be related to ΔSST, can be obtained as:

$$\Delta Q^{For}_{LWD_{\square}} = \Delta Q^{\square}_{LWD_{\square}} - \Delta Q^{Fbk}_{LWD_{\square}}$$

Total longwave feedback. The net longwave radiation flux perturbation can then be written as:

$$\Delta Q^{\square}_{LW_{\square}} = \Delta Q^{For}_{LW_{\square}} + \lambda_{LW_{\square}} \Delta SST$$

With $\Delta Q^{For}_{LW_{\square}} = \Delta Q^{For}_{LWD_{\square}}$ and $\lambda_{LW_{\square}} = \lambda_{LWD_{\square}} + \lambda_{LWU_{\square}}$.

Other feedbacks. The last two components of heat flux changes, ΔQ_{SW} and ΔQ_{SH}, are entirely considered as forcing components. Indeed, because we assume no changes in δT between the present and future climate, $\Delta Q^{Fbk}_{SH} = 0$ and $\Delta Q^{For}_{SH} = \Delta Q^{\square}_{SH}$. Similarly, ΔQ_{SW} in the tropics is strongly related to cloud changes, which cannot easily be related to local SST changes.

3.3.Heat flux changes: separating the forcing and feedback components

Building heat flux forcing perturbations. While $\Delta F(i,j,t)$ is applied as such for the wind-stress and freshwater flux, we separate the heat flux forcing change into feedback (SST-dependent) and forcing (SST-independent) components as detailed above. We first calculate the forcing component of latent (ΔQ_{LH}^{For}) and longwave heat flux perturbations ($\Delta Q_{LW_{\square}}^{For}$), which are not directly related to ΔSST, as:

$$\Delta Q_{LW_{CMIP}}^{For}(i,j,t) \;=\; \Delta Q_{LW_{CMIP}}^{\square}(i,j,t) \;-(\lambda_{LW_{CMIP}}^{\square}(i,j,t_{seas}) \;*\; \Delta \mathrm{SST}_{CMIP}(i,j,t)\;)$$

$$\Delta Q_{LH}^{For}(i,j,t) = \; \Delta Q_{LH}^{\square}(i,j,t) - (\lambda_{LH}^{IPSL}(i,j,t_{seas}) \;*\; \Delta \mathrm{SST}_{CMIP}(i,j,t))$$

where $\Delta Q_{LW_{\square}}^{\square}(i,j,t)$ and $\Delta Q_{LH}^{\square}(i,j,t)$ are the longwave and latent heat flux perturbations for the selected ESM as calculated in Section 2.2, $\lambda_{LW_{\square}}^{\square}(i,j,t_{seas})$ and $\lambda_{LH}^{\square}(i,j,t_{seas})$ are the seasonally varying feedback coefficients from the selected ESM as calculated in Section 2.3 and $\Delta SST_{CMIP}(i,j,t)$ is the anomalous SST relative to the historical period calculated in the same way as $\Delta Q(i,j,t)$. In our forced climate change simulations, the total heat flux is then formulated as:

$$\Delta Q_{tot}(i,j,t) = \; (\Delta Q_{SW} + \; \Delta Q_{SH} + \Delta Q_{LW_{\square}}^{For} + \Delta Q_{LH_{\square}}^{For})(i,j,t) - (\lambda_{tot}^{\square}(i,j,t_{seas}) * \Delta \mathrm{SST}^{CC}(i,j,t))$$

where ΔQ_{tot} is the total heat flux perturbation applied to the ocean model simulation, ΔQ_{SW} and ΔQ_{SH} are the shortwave and sensible heat fluxes perturbations directly derived from the selected ESM. The SST-dependent part of the surface heat flux changes is represented as a linear relaxation to the pre-industrial simulation SST in our CC experiments. λ_{tot} being the total negative feedback coefficient derived from the ESM outputs expressed as $\lambda_{tot} = \lambda_{LW_{\square}}^{\square} + \lambda_{LH}^{\square}$ and $\Delta \mathrm{SST}^{CC}(i,j,t)$ the SST anomalies related to climate change in our forced framework calculated as the SST difference between CC and CTL forced ocean simulations model: $\Delta \mathrm{SST}^{CC}(i,j,t) = \mathrm{SST}^{CC}(i,j,t) - \mathrm{SST}^{CTL}(i,j,t)$. feedback coefficient.

Application to the IPSL and CNRM forcing. In the following section, we will demonstrate the efficiency of this protocol by applying it to the NEMO3.6 ocean model with forcing perturbations derived from the IPSL-CM6A-LR and CNRM-ESM2-1 coupled model. The CTL experiment spans two cycles, which are representative of the 1950s background oceanic state and simulate a realistic intraseasonal to interdecadal natural variability over the 1958-2022

period, yet with the long-term trend associated with climate change removed. As schematized in Figure 6, the climate change simulation (CC-ALL) is performed over the 1958–2087 timeframe (i.e. two JRA55 cycles) to simulate the oceanic response to climate change perturbations originating from the historical and SSP585 scenarios of the selected ESM ensemble mean. CC-ALL experiment employs the same ocean-only configuration as CTL but adds all IPSL-CM6A-LR fluxes perturbations (heat, wind-stress and freshwater) to the CTL present-day fluxes. The reference period for calculating these flux perturbations spans 1948 to 1967, ensuring near-zero anomalies at the beginning of the JRA55 forcing period (1958). Wind-stress and freshwater flux perturbations are directly added to their present-day evolution from the CTL experiment. For heat fluxes perturbations, only the SST-independent part is added to CTL heat fluxes, calculated as described above. The SST-dependent part of the heat flux change is then represented as a relaxation to present day CTL SST, with the feedback coefficient computed as in section 3.2. This ensure that heat flux changes are consistent with the SST evolution in the experiment. This experimental design can however be applied to any ESM and its ocean-only configuration, provided that the externally forced historical and future response can be extracted.

4. Results

4.1. IPSL-CM6A-LR forcing perturbations

Flux perturbations patterns. Figure 7ab displays the wind-stress and freshwater flux perturbations derived from the IPSL-CM6A-LR model over the last 20 years of the CC simulation (2068-2087). These fluxes perturbations are generally representative of those in other ESMs (Shanshan et al. 2024). The total heat flux perturbations can be either positive or negative, depending on the location, because of the opposite effect of the forcing component that predominantly warms the ocean surface (Fig. 7c), largely through reduced latent cooling in response to wind speed reduction, and the online negative feedback component that counters the warming induced by the direct forcing (Fig. 7d), largely through enhanced evaporative cooling in response to surface warming through the Clausius-Clapeyron relationship.. The spatial distribution of this feedback term is closely related to the spatial distribution of the feedback coefficient (Fig. 7e), primarily determined by the latent heat flux feedback coefficient (not shown), the total longwave radiative feedback being weaker and more homogeneous. The pattern of the latent heat flux feedback coefficient is largely governed by the pattern of the present-day climatological latent heat flux (see section 3.2). In the tropics, the feedback

coefficient is maximum on either side of the equator in the three tropical basins, coinciding with regions of strong trade winds, and minimum at the equator, where climatological winds are weaker.

Flux and SST evolution. Figure 8a displays the evolution of globally-averaged heat flux perturbations derived from the coupled and ocean-only simulations over the 1958-2087 period, as well as their forcing and feedback components. By design, the forcing component is identical in both simulations. The feedback component diagnosed from the ESMs outputs and calculated online in our ocean-only simulation framework closely match. Consequently, their net heat flux perturbation (Fig. 8a) and the corresponding SST changes (Fig. 8b) are very similar. These results suggest that the ESM mean state bias correction does not affect global SST changes and that our ocean-only framework, including our online damping, can accurately reproduce the global SST evolution simulated by the coupled model. Figure 8cd presents similar diagnostics to Figure 8ab, but focuses on the Niño3 region. While the forcing perturbations are identical by design in both simulations, the damping and net heat flux perturbations are different. The damping is weaker in the ESM compared to CC-ALL experiment, leading to a larger net heat flux warming in the ESM. The SST evolution also differs between the two simulations (Fig. 8d), with the forced simulation showing enhanced warming compared to the coupled simulation. This result illustrates that the mitigation of the coupled model mean biases can lead to different regional SST responses.

4.2. Impact of IPSL-CM6A-LR biases on future projections in the tropical Pacific

Impact of bias correction in the tropical Pacific. Figure 9 highlights the differences in regional projections between the IPSL coupled model and the bias-corrected CC-ALL simulation in the tropical Pacific. Figure 9a,b shows that the ocean-only simulation qualitatively reproduces the SST pattern simulated by the coupled model, with enhanced warming in the equatorial Pacific and reduced cooling in the southeastern subtropical Pacific. However, marked regional differences, especially in the equatorial region, are evident. The ESM projects a modest relative warming over the entire equatorial band, while CC-ALL projects a larger relative warming in the eastern equatorial Pacific and a relative cooling over the western equatorial Pacific, opposite to the response of the ESM. This leads to a significant reduction in the zonal equatorial SST gradient in the ocean-only simulation, in contrast to the very modest change in the coupled simulation. These differences likely results from the strong equatorial

cold tongue bias in the IPSL-CM6A-LR model. The projected equatorial trade winds relaxation (Fig. 7b) likely acts to weaken the unrealistically strong upwelling simulated by this coupled model in the western Pacific, resulting in an enhanced warming there. In the bias-corrected simulation, the absence of upwelling in the western Pacific prevents a strong dynamical response to this wind relaxation. Differences in projected patterns are also evident for Chl and O_2. Figure 9d,e show that the ESM projects the largest Chl decrease in the western Pacific, with a smaller decrease in the eastern Pacific, while CC-ALL projects a very small decrease in the western Pacific and a much larger decrease in the central and eastern Pacific. These differences also most likely results from the strong IPSL-CM6A-LR cold tongue bias. Finally, the O_2 decrease in the equatorial Pacific projected by the ESM is significantly reduced in the ocean-only simulation (Fig. 9g,h).

Framework evaluation. These results suggest that IPSL-CM6A-LR present-day biases may strongly influence future oceanic projections, affecting both physical and biogeochemical properties. However, it is also possible that the different responses arise from inaccuracies in our ocean-only modelling framework. To test this hypothesis, we have performed a series of additional ocean-only simulations, similar to CC-ALL and CTL, but with the climatological flux biases from the IPSL-CM6A-LR added to the CTL and CC-ALL heat fluxes (Figure 6). These simulations (CTL-BIAS and CC-BIAS) demonstrate that reintroducing the coupled model biases into our ocean-only framework (middle panels of Figure 9) allow to bring the ocean model solution much closer to the coupled model results (right panels of Fig. 9) than to the debiased forced simulation (left panels of Fig. 9). This clearly demonstrates that most of the differences between the CC-ALL and the IPSL-CM6A-LR simulations can be attributed to the different background ocean state, confirming that the coupled model biases strongly alter future projections.

4.3.Process-oriented studies

Mechanisms driving the Pacific warming pattern. The proposed framework offers an alternative dynamical approach to statistical methods, such as the “emergent constraint” methods, for correcting future oceanic projections from ESMs biases. Additonally, it serves as a powerful tool for conducting process-oriented studies. Figure 6 provides a schematic of how sensitivity experiments can be used to understand the mechanisms underlying future model projections. These experiments are similar to the CC-ALL simulations, but each driven by a

single component of the flux perturbations: heat fluxes (CC-Q), wind stress (CC-τ) or freshwater fluxes (CC-F). Comparing these to CC-ALL allows us to assess the respective contribution of the flux component to future projections. As anticipated, the global warming signal is driven by heat flux perturbations (Fig. 11a), with wind stress and freshwater perturbations playing a much smaller role. However, this is different when examining the drivers of the Pacific warming patterns (Figure 11b-f). While relative cooling in the southeastern Pacific is largely due to heat flux perturbations, changes in the equatorial zonal gradient result from a combined response to the heat flux and wind-stress perturbations. The reduced damping in the eastern equatorial Pacific (Fig. 7d) and the ocean dynamical response to the relaxation of the trade winds (Fig. 7b) contribute almost equally contribute the relative warming in the eastern Pacific and relative cooling in the western Pacific. These results are put into a broader context in the discussion section.

4.4. Application to the CNRM-ESM2-1

Impact of bias correction in the tropical Pacific. To evaluate the sensitivity of our results to the ESM forcing perturbations, we conducted similar climate change simulations (CC-ALL, CC-Q, CC-T, CC-F) using fluxes perturbations derived from the CNRM-ESM2-1 projections. Since this ESM uses the same oceanic component as the IPSL-CM6A-LR model, any differences in bias-corrected projections can only be attributed to the ESM forcing perturbations applied. As shown on Figure 11b, the projected RSST pattern for the CNRM-ESM2-1 coupled model significantly differs from that of the IPSL-CM6A-LR one. While the IPSL-CM6A-LR model projects an enhanced warming all along the equatorial band (Fig. 9a). the CNRM-ESM2-1 model simulates a modest enhanced warming localised in the eastern Pacific, west of the Galapagos islands, with very weak RSST changes in the rest of the equatorial Pacific. The pattern projected by the CNRM-ESM2-1 model more closely resembles the pattern projected by most other ESMs compared to the ISPL-CM6A-LR. When correcting for the CNRM-ESM2-1 biases, the enhanced warming extends all over the central and eastern equatorial Pacific and the equatorial western Pacific experiences a relative cooling (Fig. 11a). Interestingly, this bias-corrected pattern resembles the one simulated with the IPSL-CM6A-LR perturbations, suggesting that our bias-correction strategy may not only impact the projected pattern but may also reduce the uncertainty across ESMs. Chl and O_2 pattern projected by the CNRM-ESM2-1 coupled and forced simulations are relatively similar to that of the IPSL-CM6A-LR model (not shown).

Driving mechanisms. Sensitivity experiments where each flux perturbation is applied individually (CC-Q, CC-T, CC-F) reveal that the same mechanisms drive the tropical Pacific warming pattern for the both bias-corrected CNRM (Fig. 11cd) and IPSL (Fig. 10de) simulations. Specifically, heat flux and wind-stress perturbations contribute similarly to the reduction of the east-west equatorial SST gradient.

5. Summary, discussion and perspectives

5.1. Summary

This paper proposes an ocean-only dynamical framework to mitigate the influence present-day biases of Earth System Models (ESMs) on future regional ocean physical and biogeochemical projections. Initially, a control experiment is conducted using fluxes derived from an atmospheric reanalysis, excluding climate change signals. Subsequently, a climate change simulation is performed by adding historical and future fluxes perturbations from a selected ESM to these background realistic fluxes. Since part of the ESM surface heat fluxes perturbation is a direct feedback to the sea surface temperature (SST) warming, these fluxes perturbations are split into SST-dependent and independent components. The climate change simulation is forced by the independent component, while the SST-dependent component is modeled online as an SST relaxation to the control experiment, accounting for Newtonian cooling and long-wave radiative feedback.

This approach demonstrates that ESMs present-day biases can heavily impact the reliability of regional physical and biogeochemical ocean projections. For instance, the strong cold-tongue bias simulated by the IPSL-CM6A-LR model causes greater warming and chlorophyll decrease in the western than in the eastern equatorial Pacific, while our bias-corrected simulation shows opposite projected patterns. Sensitivity experiments applying heat, freshwater and momentum fluxes perturbations separately further indicate that thermodynamical and dynamical processes equally contribute to this warming pattern, highlighting the strong role of the Bjerknes feedback. This cost-effective method can be applied to any ESMs ocean component to produce more reliable regional oceanic projections and understand the mechanisms driving the projected patterns.

5.2. Discussion

Comparison with a bulk-forced approach. Our efficient flux-forced simulation strategy may appear somewhat complex, leading to questions whether a simpler strategy, where the ocean model is forced by surface atmospheric perturbations from ESMs added to JRA55 detrended forcing, might yield similar results. Figure 11 however illustrates that bias-corrected projected RSST patterns differ when using the flux-forced strategy detailed in this paper (Fig. 11a) and a simpler bulk-forced approach (Fig. 11b). The bulk-forced approach simulates an enhanced warming over most of the equatorial Pacific, closely resembling the pattern simulated by the IPSL-CM6A-LR coupled model (Fig. 11c). This similarity is likely due to the fact that the bulk-corrected warming pattern is strongly driven towards the coupled model projected SST patterns by incorporating near surface humidity and air temperature perturbations simulated by the coupled model in the bulk formulae. In contrast, a flux-forced strategy using an online SST damping constrains less the forced solution towards the one of the coupled model.

Comparison with previous approaches. To the authors' knowledge, only a single study (Matear et al. 2015) has attempted to assess the impact of ESMs oceanic biases onto future projections in a dynamical ocean-only framework. Their study focused specifically on the Western Pacific Ocean. However, their approach differed significantly from ours: they applied their bias-correction strategy using a different ocean model with considerably higher horizontal resolution than the coupled model they used for comparison. Consequently, they were unable to isolate the effects of bias correction from those of resolution enhancement or the use of a different model, unlike our framework. Their study concluded that while enhanced spatial resolution and bias correction together had only a marginal impact on physical oceanic projections, they strongly influenced the phytoplankton response. Despite both studies employing a flux-forced approach, direct comparison with our study is challenging due to differences in climate change simulations strategies (time-slice vs. transient simulations), the impossibility to cleanly isolate the impact of bias correction in their framework or the different coupled models analyzed.

5.3.Perspectives

Framework improvements. Our preliminary results with the IPSL-CM6A-LR and CNRM-ESM2-1 models suggest that ESMs oceanic biases can heavily impact the reliability of

future projections but also contribute to projections uncertainties. Expanding our framework to encompass a broader range of ESMs would enable a more comprehensive assessment of how biases inherent in different ESMs affect projection biases and uncertainties. It may also be interesting to assess the feasibility of deriving feedback coefficient directly from observational data, which introduces an additional layer of bias correction to assess the sensitivity of global warming levels and patterns projected by ESMs to these feedback biases. Moreover, tropical and subtropical cloud changes and their shortwave radiative effect projected by ESMs has also been identify as a major driver of the uncertainty in global warming level (Andrews et al., 2012; Vial et al., 2013) but also regional warming patterns (Ying et al., 2016). In our current framework, tropical shortwave changes are considered entirely as a forcing because these changes are not directly related to local SST changes but rather to relative SST changes through the warmer-get-wetter mechanisms. Including shortwave feedback through RSST in our modelling framework would allow to investigate the sensitivity of global and regional SST changes to cloud feedback uncertainties. On a longer term, it may also be useful to implement a flux-correction strategy in a fully coupled ocean-atmosphere coupled model to allow accounting for coupled feedbacks other that those directly related to local SST changes (e.g. circulation changes) on the projected SST changes. This coupled framework will not only provide a refine assessment of the impact of ESMs biases on projected changes in the ocean but also in the atmosphere, allowing for instance to address the issue of the uncertain response of the Walker Cell to climate change (Chung et al. 2019; Heede et al. 2021).

Assessing underlying mechanisms. The framework presented in this study provides a comprehensive tool for elucidating the drivers behind the heterogeneous tropical SST responses to climate change, which are crucial for understanding associated changes in tropical rainfall and circulation patterns. The projected SST patterns in the tropical Pacific are influenced by a combination of thermodynamic and dynamical processes. Thermodynamically, enhanced evaporative damping over the warm pool (Xie et al., 2010; Zhang and Li, 2014) and differential cloud-radiation feedbacks play significant roles (Ramanathan and Collins, 1991; Erfani et al., 2019) in shaping the SST gradient across the basin. Dynamically, processes such as the ocean thermostat mechanism and the Bjerknes feedback further modulate these SST patterns. Our preliminary results indicate that heat flux changes and the dynamical ocean response to equatorial trade winds relaxation both contribute to shape the El Niño-like warming pattern in the tropical Pacific. Extending this analysis to other ESMs would provide insights into model-specific responses and their implications for future climate projections. Moreover, additional

sensitivity experiments could provide a refined assessment of the specific contribution of individual processes. For example, applying a spatially uniform latent heat feedback coefficient would allow isolating the role of evaporative cooling effects on the El Niño-like warming pattern, while experiments combining uniform coefficients and heat flux perturbations, and excluding wind stress and freshwater fluxes, could elucidate the specific contribution of the ocean thermostat mechanism on the tropical Pacific warming pattern. Beyond the tropical Pacific, this framework can allow identifying how ocean dynamical changes and thermodynamical processes contribute to the Indian Ocean Dipole (IOD)-like warming (Zhang and Li, 2014; Sharma et al., 2023) and the equatorial El Niño-like warming pattern in the equatorial Atlantic. Furthermore, this framework will allow to understand the processes driving the regional biogeochemical response, including the respective role of increased upper ocean stratification versus changes in ocean dynamics in projected chlorophyll concentrations declines or the respective contribution of physical (solubility, ventilation) and biological (respiration) processes on the projected O_2 changes at depth.

In conclusion, this framework represents a powerful approach for improving the accuracy of regional oceanic projections for both their physical and biogeochemical properties but also to advance our understanding of their underlying processes.

Acknowlegements.

References:

References:

Adachi, S. A., & Tomita, H. (2020). Methodology of the constraint condition in dynamical downscaling for regional climate evaluation: A review. *Journal of Geophysical Research: Atmospheres*, *125*(11), e2019JD032166.

Almendra, I., Dewitte, B., Garçon, V., Muñoz, P., Parada, C., Montes, I., ... & Oschlies, A. (2024). Emergent constraint on oxygenation of the upper South Eastern Pacific oxygen minimum zone in the twenty-first century. *Communications Earth & Environment*, *5*(1), 284.

Andrews, T., Gregory, J. M., Webb, M. J., & Taylor, K. E. (2012). Forcing, feedbacks and climate sensitivity in CMIP5 coupled atmosphere-ocean climate models. *Geophysical research letters*, *39*(9).

Andrews, T., Gregory, J. M., Paynter, D., Silvers, L. G., Zhou, C., Mauritsen, T., ... & Titchner, H. (2018). Accounting for changing temperature patterns increases historical estimates of climate sensitivity. *Geophysical Research Letters*, *45*(16), 8490-8499.

Aumont, O., Éthé, C., Tagliabue, A., Bopp, L., & Gehlen, M. (2015). PISCES-v2: an ocean biogeochemical model for carbon and ecosystem studies. *Geoscientific Model Development Discussions*, *8*(2), 1375-1509.

Bayr, T., Dommenget, D., Martin, T., & Power, S. B. (2014). The eastward shift of the Walker Circulation in response to global warming and its relationship to ENSO variability. *Climate dynamics*, *43*, 2747-2763.

Beobide-Arsuaga, G., Bayr, T., Reintges, A., & Latif, M. (2021). Uncertainty of ENSO-amplitude projections in CMIP5 and CMIP6 models. *Climate Dynamics*, *56*, 3875-3888.

Bindoff, N. L. et al. (2019). Changing ocean, marine ecosystems, and dependent communities.

Bjerknes, J. (1969). Atmospheric teleconnections from the equatorial Pacific. *Monthly weather review*, *97*(3), 163-172.

Bopp, L., Resplandy, L., Orr, J. C., Doney, S. C., Dunne, J. P., Gehlen, M., ... & Vichi, M. (2013). Multiple stressors of ocean ecosystems in the 21st century: projections with CMIP5 models. *Biogeosciences*, *10*(10), 6225-6245.

Boucher, O., Servonnat, J., Albright, A. L., Aumont, O., Balkanski, Y., Bastrikov, V., ... & Vuichard, N. (2020). Presentation and evaluation of the IPSL-CM6A-LR climate model. *Journal of Advances in Modeling Earth Systems*, *12*(7), e2019MS002010.

Cabré, A., Marinov, I., Bernardello, R., & Bianchi, D. (2015). Oxygen minimum zones in the tropical Pacific across CMIP5 models: mean state differences and climate change trends. *Biogeosciences*, *12*(18), 5429-5454.

Cai, W., & Cowan, T. (2013). Why is the amplitude of the Indian Ocean Dipole overly large in CMIP3 and CMIP5 climate models?. *Geophysical Research Letters*, *40*(6), 1200-1205.

Cai, W., Borlace, S., Lengaigne, M., Van Rensch, P., Collins, M., Vecchi, G., ... & Jin, F. F. (2014). Increasing frequency of extreme El Niño events due to greenhouse warming. *Nature climate change*, *4*(2), 111-116.

Cai, W., Zheng, X. T., Weller, E., Collins, M., Cowan, T., Lengaigne, M., ... & Yamagata, T. (2013). Projected response of the Indian Ocean Dipole to greenhouse warming. *Nature geoscience*, *6*(12), 999-1007.

Chung, E. S., Timmermann, A., Soden, B. J., Ha, K. J., Shi, L., & John, V. O. (2019). Reconciling opposing Walker circulation trends in observations and model projections. *Nature Climate Change*, *9*(5), 405-412.

Clement, A. C., Seager, R., Cane, M. A., & Zebiak, S. E. (1996). An ocean dynamical thermostat. *Journal of Climate*, *9*(9), 2190-2196.

Collins, M. (2005). El Niño-or La Niña-like climate change?. *Climate Dynamics*, *24*, 89-104.

DiNezio, P. N., Clement, A. C., Vecchi, G. A., Soden, B. J., Kirtman, B. P., & Lee, S. K. (2009). Climate response of the equatorial Pacific to global warming. *Journal of Climate*, *22*(18), 4873-4892.

Dong, Y., Armour, K. C., Zelinka, M. D., Proistosescu, C., Battisti, D. S., Zhou, C., & Andrews, T. (2020). Intermodel spread in the pattern effect and its contribution to climate sensitivity in CMIP5 and CMIP6 models. *Journal of Climate*, *33*(18), 7755-7775.

Erfani, E., & Burls, N. J. (2019). The strength of low-cloud feedbacks and tropical climate: A CESM sensitivity study. *Journal of Climate*, *32*(9), 2497-2516.

Eyring, V., Cox, P. M., Flato, G. M., Gleckler, P. J., Abramowitz, G., Caldwell, P., ... & Williamson, M. S. (2019). Taking climate model evaluation to the next level. *Nature Climate Change*, *9*(2), 102-110.

Fu, W., Randerson, J. T., & Moore, J. K. (2016). Climate change impacts on net primary production (NPP) and export production (EP) regulated by increasing stratification and phytoplankton community structure in the CMIP5 models. *Biogeosciences*, *13*(18), 5151-5170.

Gregory, J. M., Bouttes, N., Griffies, S. M., Haak, H., Hurlin, W. J., Jungclaus, J., ... & Winton, M. (2016). The Flux-Anomaly-Forced Model Intercomparison Project (FAFMIP) contribution to CMIP6: Investigation of sea-level and ocean climate change in response to CO 2 forcing. *Geoscientific Model Development*, *9*(11), 3993-4017.

Hall, A., Cox, P., Huntingford, C., & Klein, S. (2019). Progressing emergent constraints on future climate change. *Nature Climate Change*, *9*(4), 269-278.

Heede, U. K., & Fedorov, A. V. (2021). Eastern equatorial Pacific warming delayed by aerosols and thermostat response to CO2 increase. *Nature Climate Change*, *11*(8), 696-703.

Held, I. M., & Soden, B. J. (2006). Robust responses of the hydrological cycle to global warming. *Journal of climate*, *19*(21), 5686-5699.

Hourdin, F., Rio, C., Grandpeix, J. Y., Madeleine, J. B., Cheruy, F., Rochetin, N., ... & Ghattas, J. (2020). LMDZ6A: The atmospheric component of the IPSL climate model with improved and better tuned physics. *Journal of Advances in Modeling Earth Systems*, *12*(7), e2019MS001892.

Huang, P., & Ying, J. (2015). A multimodel ensemble pattern regression method to correct the tropical Pacific SST change patterns under global warming. *Journal of Climate*, *28*(12), 4706-4723.

Knutti, R., Sedláček, J., Sanderson, B. M., Lorenz, R., Fischer, E. M., & Eyring, V. (2017). A climate model projection weighting scheme accounting for performance and interdependence. *Geophysical Research Letters*, *44*(4), 1909-1918.

Kobayashi, S., Ota, Y., Harada, Y., Ebita, A., Moriya, M., Onoda, H., ... & Takahashi, K. (2015). The JRA-55 reanalysis: General specifications and basic characteristics. *Journal of the Meteorological Society of Japan. Ser. II*, *93*(1), 5-48.

Krinner, G., Viovy, N., de Noblet-Ducoudré, N., Ogée, J., Polcher, J., Friedlingstein, P., Ciais, P., Sitch, S., and Prentice, I. C.: A dynamic global vegetation model for studies of the coupled atmosphere-biosphere system: Dvgm for coupled climate studies, Global Biogeochem. Cy., 19, GB1015, https://doi.org/10.1029/2003GB002199, 2005.

Kwiatkowski, L., Bopp, L., Aumont, O., Ciais, P., Cox, P. M., Laufkötter, C., ... & Séférian, R. (2017). Emergent constraints on projections of declining primary production in the tropical oceans. *Nature Climate Change*, *7*(5), 355-358.

Kwiatkowski, L., Aumont, O., & Bopp, L. (2019). Consistent trophic amplification of marine biomass declines under climate change. *Global change biology*, *25*(1), 218-229.

Kwiatkowski, L. et al. (2020). Twenty-first century ocean warming, acidification, deoxygenation, and upper-ocean nutrient and primary production decline from CMIP6 model projections. *Biogeosciences*, *17*(13), 3439-3470.

Li, G., Xie, S. P., Du, Y., & Luo, Y. (2016). Effects of excessive equatorial cold tongue bias on the projections of tropical Pacific climate change. Part I: The warming pattern in CMIP5 multi-model ensemble. *Climate Dynamics*, *47*, 3817-3831.

Li, G., Xie, S. P., & Du, Y. (2016). A robust but spurious pattern of climate change in model projections over the tropical Indian Ocean. *Journal of Climate*, *29*(15), 5589-5608.

Liu, Z., Vavrus, S., He, F., Wen, N., & Zhong, Y. (2005). Rethinking tropical ocean response to global warming: The enhanced equatorial warming. *Journal of Climate*, *18*(22), 4684-4700.

Lotze, H. K., Tittensor, D. P., Bryndum-Buchholz, A., Eddy, T. D., Cheung, W. W., Galbraith, E. D., ... & Worm, B. (2019). Global ensemble projections reveal trophic amplification of ocean biomass declines with climate change. *Proceedings of the National Academy of Sciences*, *116*(26), 12907-12912.

Luo, J. J., Wang, G., & Dommenget, D. (2018). May common model biases reduce CMIP5's ability to simulate the recent Pacific La Niña-like cooling?. *Climate Dynamics*, *50*, 1335-1351.

Ma, J., & Xie, S. P. (2013). Regional patterns of sea surface temperature change: A source of uncertainty in future projections of precipitation and atmospheric circulation. *Journal of climate*, *26*(8), 2482-2501.

Madec, G., Bourdallé-Badie, R., Bouttier, P. A., Bricaud, C., Bruciaferri, D., Calvert, D., ... & Vancoppenolle, M. (2017). NEMO ocean engine.

Masson-Delmotte et al. (2021). Climate change 2021: the physical science basis. *Contribution of working group I to the sixth assessment report of the intergovernmental panel on climate change*, *2*(1), 2391.

Matear, R. J., Chamberlain, M. A., Sun, C., & Feng, M. (2015). Climate change projection for the western tropical Pacific Ocean using a high-resolution ocean model: Implications for tuna fisheries. *Deep Sea Research Part II: Topical Studies in Oceanography*, *113*, 22-46.

Oschlies, A., Brandt, P., Stramma, L., & Schmidtko, S. (2018). Drivers and mechanisms of ocean deoxygenation. *Nature Geoscience*, *11*(7), 467-473.

Pandolfi, J. M., Connolly, S. R., Marshall, D. J., & Cohen, A. L. (2011). Projecting coral reef futures under global warming and ocean acidification. *science*, *333*(6041), 418-422.

Pendergrass, A. G., Conley, A., & Vitt, F. M. (2018). Surface and top-of-atmosphere radiative feedback kernels for CESM-CAM5. *Earth System Science Data*, *10*(1), 317-324.

Power, S., Lengaigne, M., Capotondi, A., Khodri, M., Vialard, J., Jebri, B., ... & Henley, B. J. (2021). Decadal climate variability in the tropical Pacific: Characteristics, causes, predictability, and prospects. *Science*, *374*(6563), eaay9165.

Ramanathan, V., & Collins, W. (1991). Thermodynamic regulation of ocean warming by cirrus clouds deduced from observations of the 1987 El Niño. *Nature*, *351*(6321), 27-32.

Richter, I., & Tokinaga, H. (2020). An overview of the performance of CMIP6 models in the tropical Atlantic: mean state, variability, and remote impacts. *Climate Dynamics*, *55*(9), 2579-2601.

Rousset, C., Vancoppenolle, M., Madec, G., Fichefet, T., Flavoni, S., Barthélemy, A., ... & Vivier, F. (2015). The Louvain-La-Neuve sea ice model LIM3. 6: global and regional capabilities. *Geoscientific Model Development*, *8*(10), 2991-3005.

Sanderson, B. M., Pendergrass, A., Koven, C. D., Brient, F., Booth, B. B., Fisher, R. A., & Knutti, R. (2021). On structural errors in emergent constraints. *Earth System Dynamics Discussions*, *2021*, 1-30.

Seager, R., Cane, M., Henderson, N., Lee, D. E., Abernathey, R., & Zhang, H. (2019). Strengthening tropical Pacific zonal sea surface temperature gradient consistent with rising greenhouse gases. *Nature Climate Change*, *9*(7), 517-522.

Séférian, R., Nabat, P., Michou, M., Saint-Martin, D., Voldoire, A., Colin, J., ... & Madec, G. (2019). Evaluation of CNRM Earth system model, CNRM-ESM2-1: Role of Earth system processes in present-day and future climate. *Journal of Advances in Modeling Earth Systems*, *11*(12), 4182-4227.

Shakespeare, C. J., & Roderick, M. L. (2022). Diagnosing instantaneous forcing and feedbacks of downwelling longwave radiation at the surface: A simple methodology and its application to CMIP5 models. *Journal of Climate*, *35*(12), 3785-3801.

Sharma, S., Ha, K. J., Yamaguchi, R., Rodgers, K. B., Timmermann, A., & Chung, E. S. (2023). Future Indian Ocean warming patterns. *Nature Communications*, *14*(1), 1789.

Sherwood, S. C., Webb, M. J., Annan, J. D., Armour, K. C., Forster, P. M., Hargreaves, J. C., ... & Zelinka, M. D. (2020). An assessment of Earth's climate sensitivity using multiple lines of evidence. *Reviews of Geophysics*, *58*(4), e2019RG000678.

Silvy, Y., Rousset, C., Guilyardi, E., Sallée, J. B., Mignot, J., Ethé, C., & Madec, G. (2022). A modeling framework to understand historical and projected ocean climate change in large coupled ensembles. *Geoscientific Model Development*, *15*(20), 7683-7713.

Sobel, A. H., Lee, C. Y., Bowen, S. G., Camargo, S. J., Cane, M. A., Clement, A., ... & Tippett, M. K. (2023). Near-term tropical cyclone risk and coupled Earth system model biases. *Proceedings of the National Academy of Sciences*, *120*(33), e2209631120.

Stevens, B., Sherwood, S. C., Bony, S., & Webb, M. J. (2016). Prospects for narrowing bounds on Earth's equilibrium climate sensitivity. *Earth's Future*, *4*(11), 512-522.

Tagliabue, A., Kwiatkowski, L., Bopp, L., Butenschön, M., Cheung, W., Lengaigne, M., & Vialard, J. (2021). Persistent uncertainties in ocean net primary production climate change projections at regional scales raise challenges for assessing impacts on ecosystem services. *Frontiers in Climate*, *3*, 738224.

Tebaldi, C., & Knutti, R. (2007). The use of the multi-model ensemble in probabilistic climate projections. *Philosophical transactions of the royal society A: mathematical, physical and engineering sciences*, *365*(1857), 2053-2075.

Terhaar, J., Frölicher, T. L., & Joos, F. (2022). Observation-constrained estimates of the global ocean carbon sink from Earth system models. *Biogeosciences*, *19*(18), 4431-4457.

Vecchi, G. A., & Soden, B. J. (2007). Global warming and the weakening of the tropical circulation. *Journal of Climate*, *20*(17), 4316-4340.

Vial, J., Dufresne, J. L., & Bony, S. (2013). On the interpretation of inter-model spread in CMIP5 climate sensitivity estimates. *Climate Dynamics*, *41*, 3339-3362.

Webb, M. J., Andrews, T., Bodas-Salcedo, A., Bony, S., Bretherton, C. S., Chadwick, R., ... & Watanabe, M. (2017). The cloud feedback model intercomparison project (CFMIP) contribution to CMIP6. *Geoscientific Model Development*, *10*(1), 359-384.

Xie, S. P., Deser, C., Vecchi, G. A., Ma, J., Teng, H., & Wittenberg, A. T. (2010). Global warming pattern formation: Sea surface temperature and rainfall. *Journal of Climate*, *23*(4), 966-986.

Yang, Y., Wu, L., Cai, W., Jia, F., Ng, B., Wang, G., & Geng, T. (2022). Suppressed Atlantic Niño/Niña variability under greenhouse warming. *Nature Climate Change*, *12*(9), 814-821.

Yeh, S. W., Cai, W., Min, S. K., McPhaden, M. J., Dommenget, D., Dewitte, B., ... & Kug, J. S. (2018). ENSO atmospheric teleconnections and their response to greenhouse gas forcing. *Reviews of Geophysics*, *56*(1), 185-206.

Ying, J., Huang, P., & Huang, R. (2016). Evaluating the formation mechanisms of the equatorial Pacific SST warming pattern in CMIP5 models. *Advances in Atmospheric Sciences*, *33*, 433-441.

Zhang, L., & Li, T. (2014). A simple analytical model for understanding the formation of sea surface temperature patterns under global warming. *Journal of Climate*, *27*(22), 8413-8421.

Zheng, X. T., Xie, S. P., Lv, L. H., & Zhou, Z. Q. (2016). Intermodel uncertainty in ENSO amplitude change tied to Pacific Ocean warming pattern. *Journal of Climate*, *29*(20), 7265-7279.

Figures:

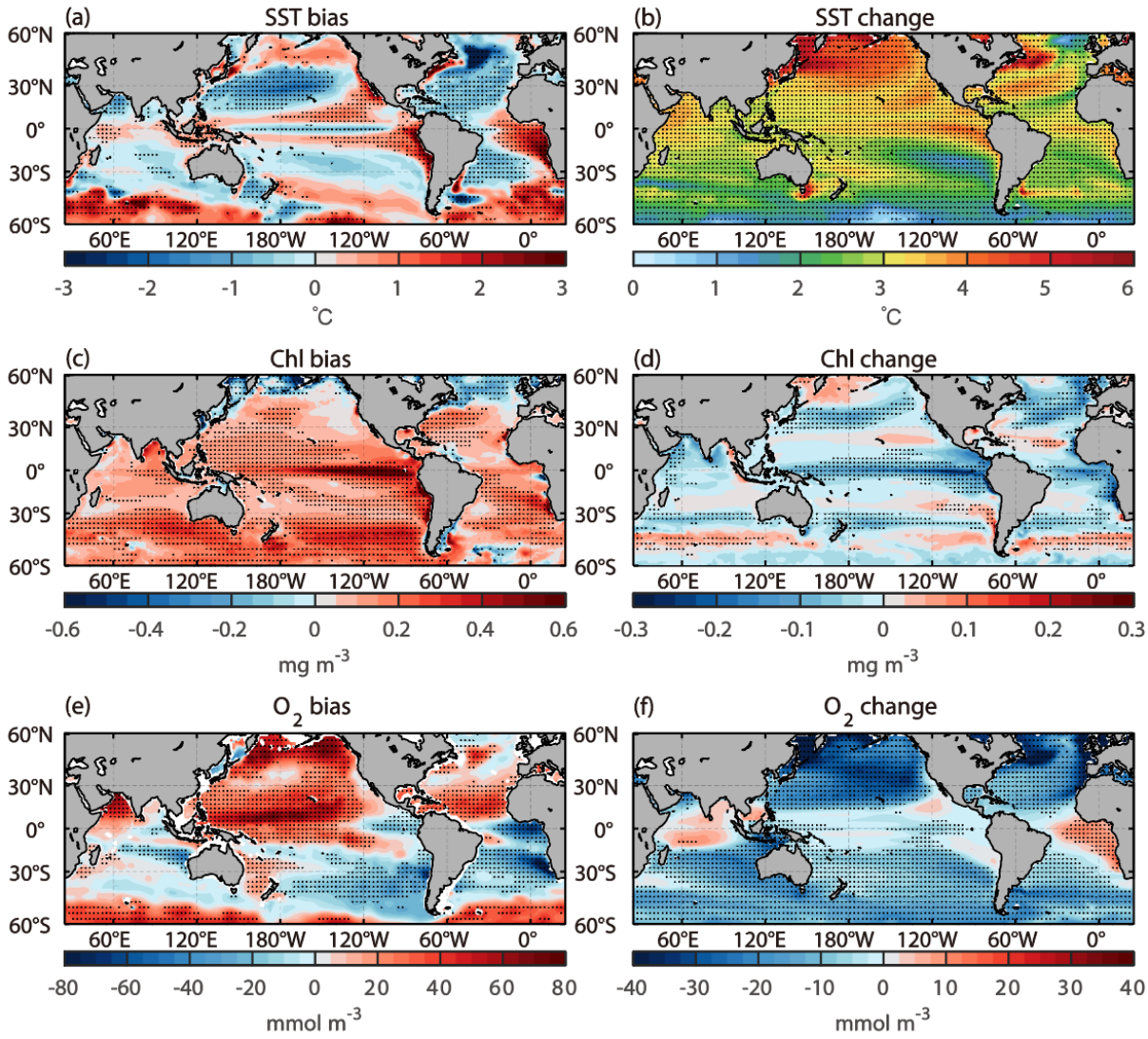

Figure 1: MMM CMIP model biases and projected changes. CMIP6 multimodel mean (MMM) bias (left) and future changes (right) for SST (top; °C), surface Chl (middle; $mg.m^{-3}$) and O_2 averaged between 200 and 800m (bottom; $mmol.m^{-3}$). The MMM is derived as the average of the first available member of the 23 CMIP models for which SST, Chl and O2 data are available are considered to calculate (see list in SI). Present-day values are defined as the 1985–2014 average of historical simulations. Changes are defined as the difference between the 2071–2100 average under SSP585 and present-day values. Future changes are defined as the difference between SSP585 simulations over the 2068-2087 period minus the historical simulations over the 1948-1967 period. Dots indicate regions where 75% of the models agree with the sign of the MMM bias or change.

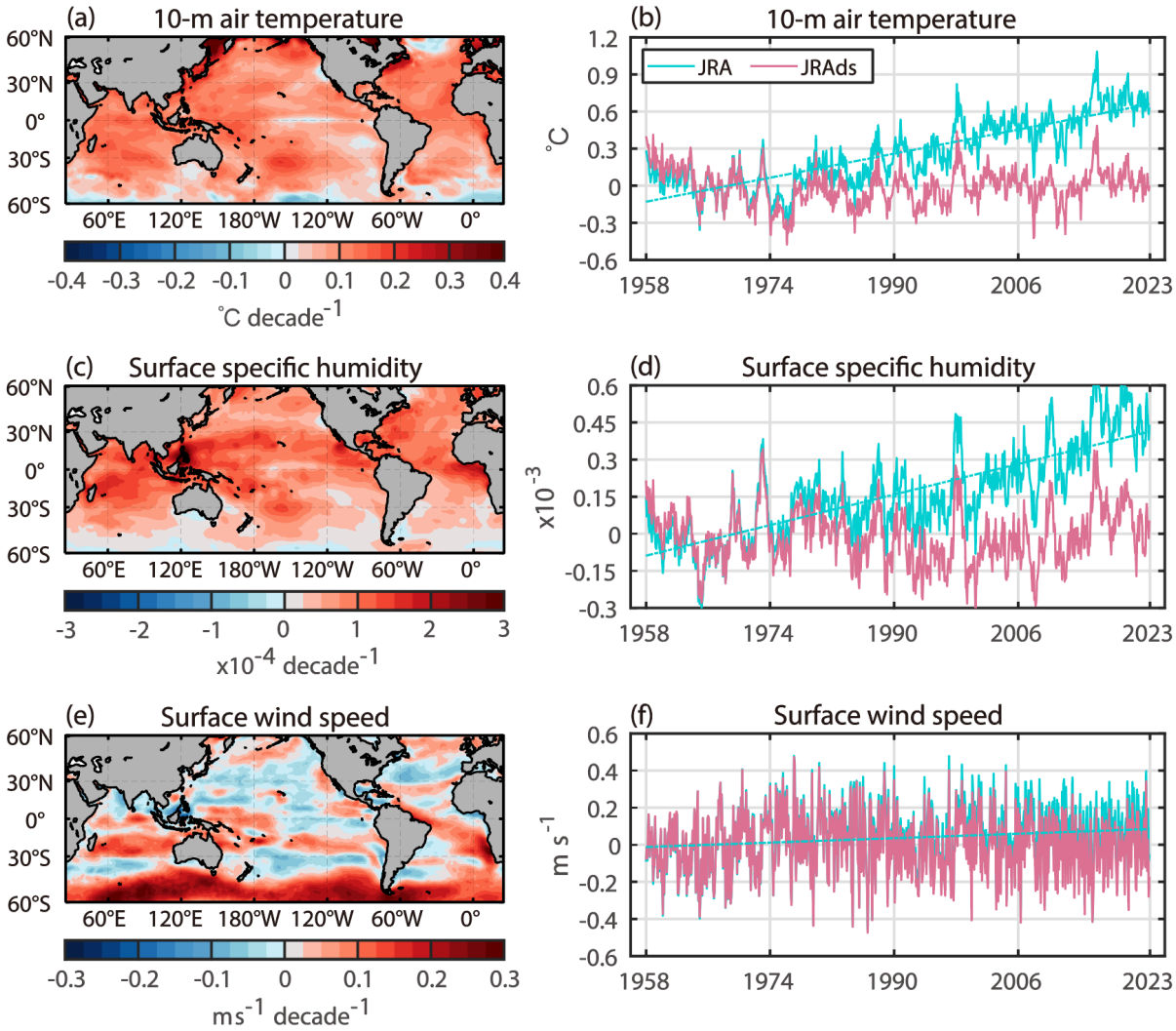

Figure 2: Detrended reanalysis forcing. Linear trend maps (left) and globally averaged original and detrended time series (right) of 10m atmospheric temperature (top), surface specific humidity (middle) and wind-speed (top) derived from JRA-55 reanalysis data over the period 1958-2022. To perform oceanic experiments that incorporate projected air-sea flux changes from CMIP historical and future simulations, it is necessary to remove the climate change signal from our control simulation. The detrended JRA dataset will be used for this purpose.

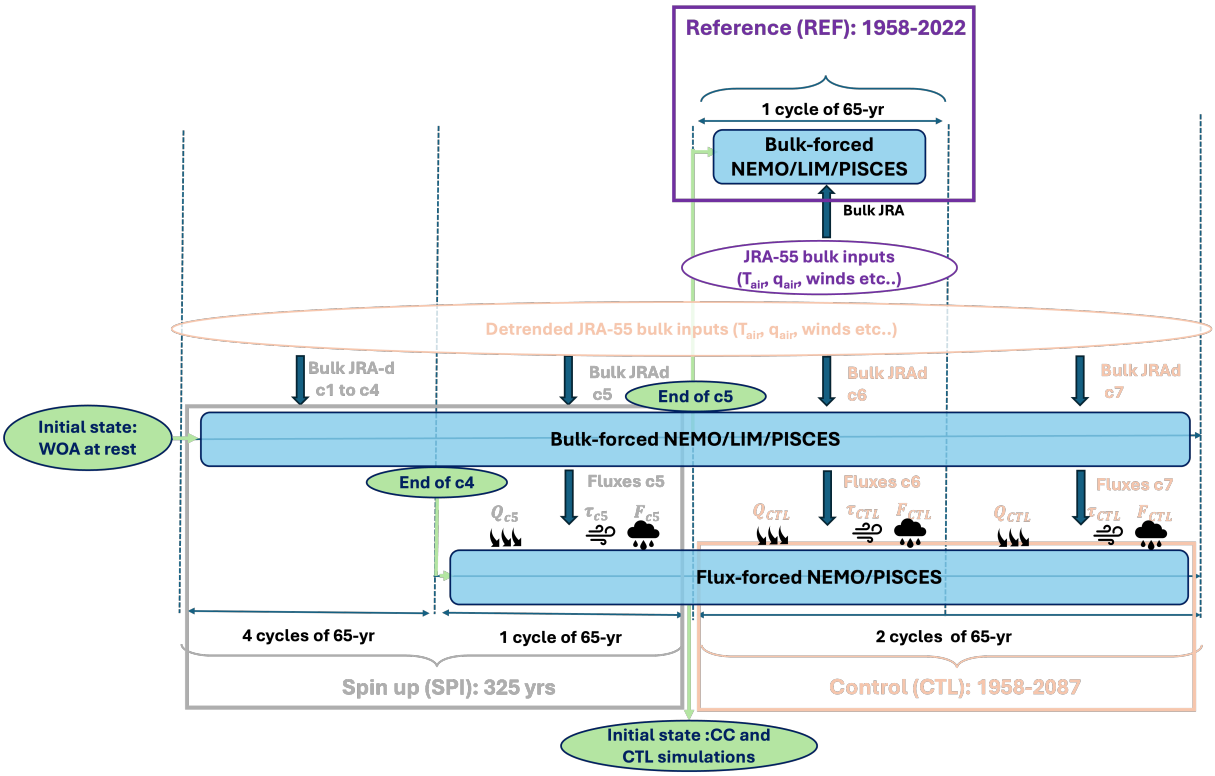

Figure 3: Schematic of spin-up and control simulations.

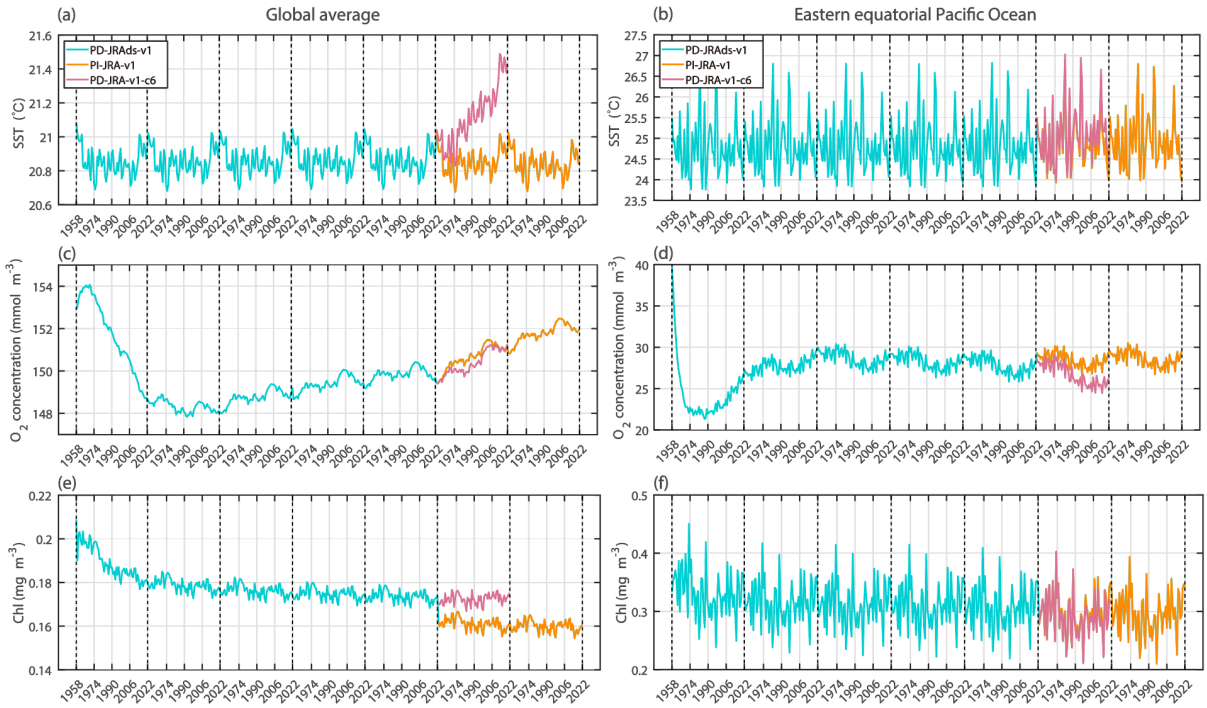

Figure 4: Control and reference simulations. Time series for SST (top; °C), surface Chl (middle; mg.m^{-3}) and O_2 averaged between 200 and 800m (bottom; mmol.m^{-3}) for three simulations: the bulk-forced spin-up simulation (SPI; grey lines), the bulk-forced and flux-forced control simulations (CTL-BULK and CTL; grey and orange lines) and the bulk-forced reference simulation (REF; pink lines). The left panels show the global averages, while the right panels focus on the Niño3 region. Detailed setups for these simulations are provided in Figure 2.

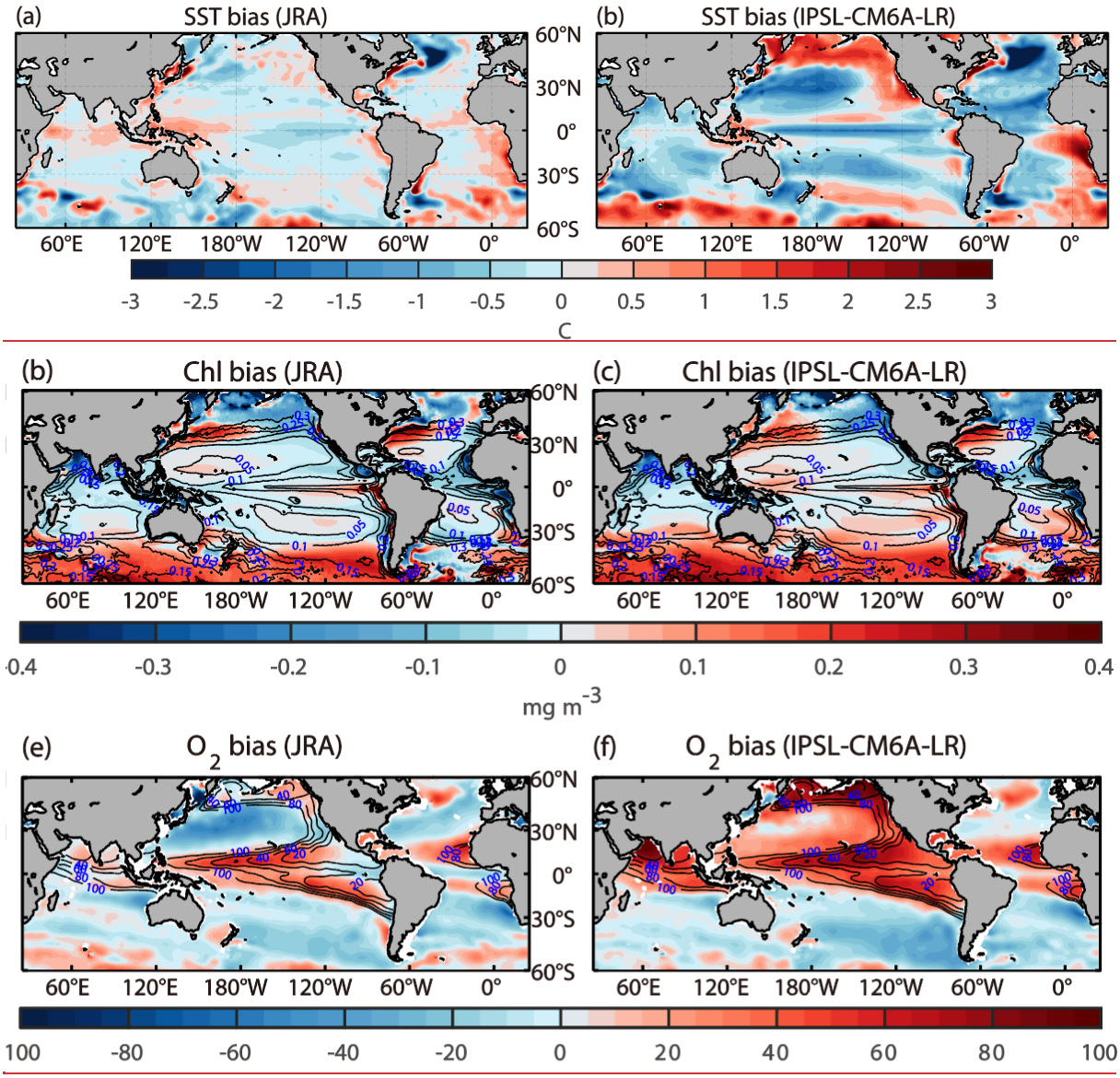

Figure 5: Climatological biases in forced and coupled ocean configurations. Global maps of climatological biases (shading) and present-day values (contours) for REF ocean-only simulation (left) and IPSL-CM6-LR historical MMM (right) for SST (top; °C), surface Chl (middle; mg.m^{-3}) and O_2 averaged between 200 and 800m (bottom; mmol.m^{-3}).

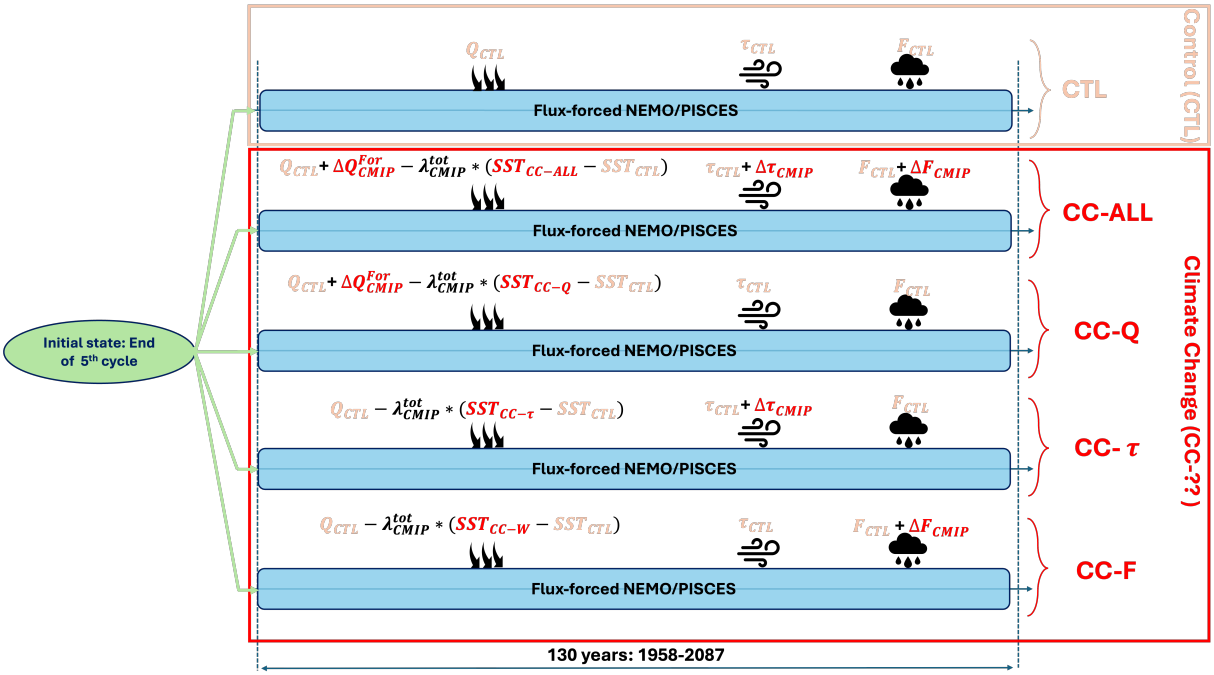

Figure 6: Schematic of control and climate change simulations

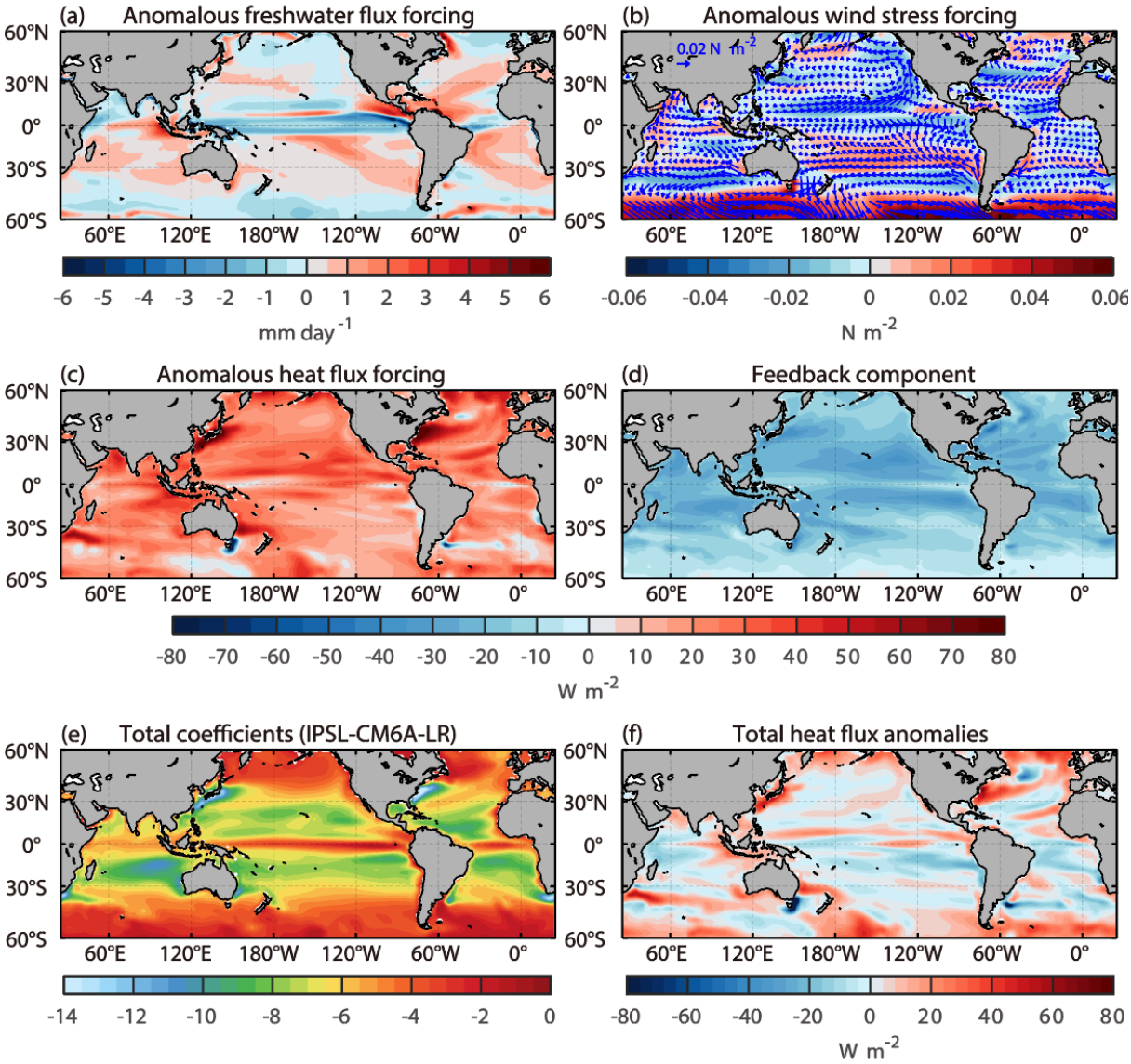

Figure 7: Forcing patterns of IPSL-CM6A-LR climate change simulations. Global maps of climate change simulations forcing over the period 2068-2087. The anomalous fluxes perturbations derived from the IPSL-CM6A-LR historical+SSP585 multi-ensemble-mean and used to force the climate change (CC-) simulations are (a) freshwater flux (mm.day-1), (b) wind-stress ($N.m^{-2}$) and (c) heat flux forcing ($W.m^{-2}$) and of (d) the online negative heat flux feedback term of CC-ALL simulation ($W.m^{-2}$) and (e) total net heat flux into the ocean difference between CC-ALL and CTL simulation ($W.m^{-2}$). (f) Global map total heat flux damping coefficient from the IPSL-CM6A-LR model ($W.m^{-2}.°C^{-1}$).

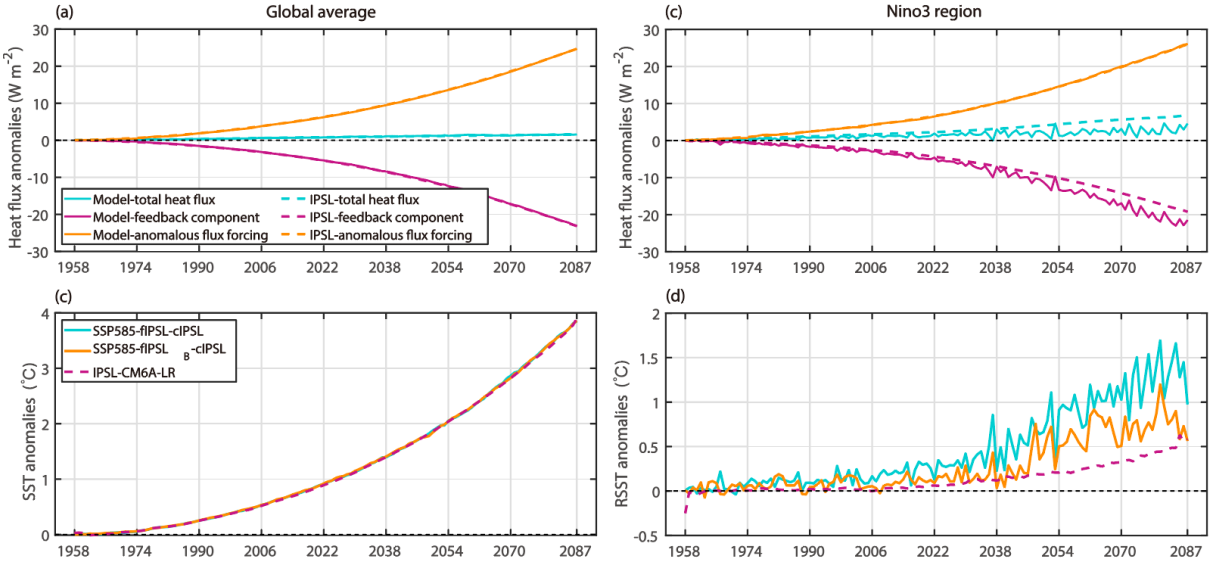

Figure 8: Forcing time evolution of IPSL-CM6A-LR climate change simulations. Time-series of total net heat flux (blue curve), feedback (pink curve) and forcing (orange curve) components ($W.m^{-2}$) for CC simulation relative to CTL simulation (plain lines) and IPSL-CM6A-LR historical+SSP585 MMM (dashed lines) relative to the period 1948-1967. (Bottom) SST anomalies (°C) of CC-ALL and CC-BIAS relative to their corresponding control simulation (dashed blue curve) and the IPSL-CM6A-LR historical+SSP585 multi-ensemble-mean simulation (orange curve) relative to the period 1948-1967. The left panels display globally averaged time series, while the right panels focus on the Niño3 region.

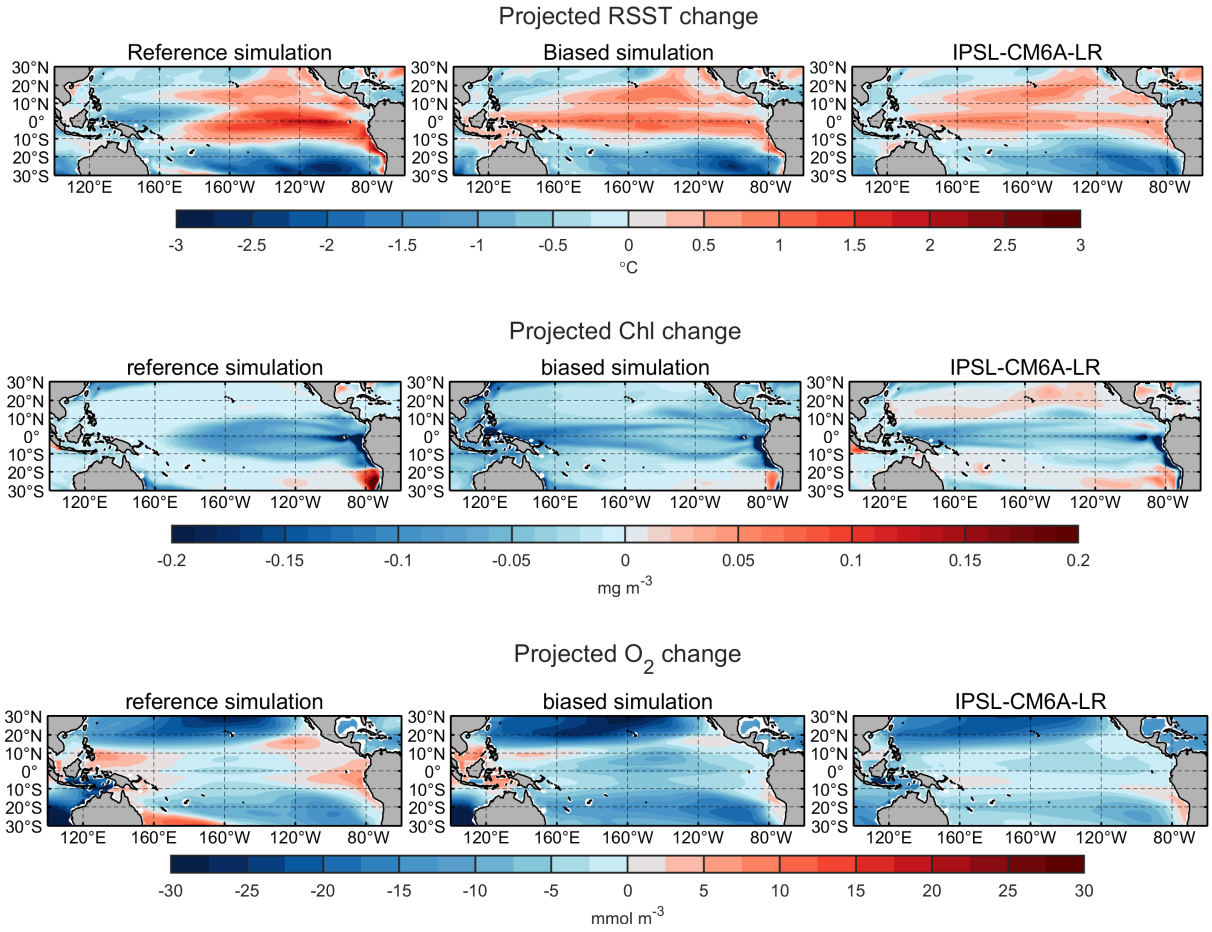

Figure 9: Impact of IPSL-CM6A-LR biases on projected changes. Tropical Pacific maps of RSST (top; °C), surface Chl (middle; mg.m^{-3}) and O_2 averaged between 200 and 800m (bottom; mmol.m^{-3}). The left panels display the difference between CC-ALL and CTL (2068-2087), the middle panel the difference between CC-BIAS and PI-BIAS (2068-2087) period and (right) the IPSL-CM6A-LR difference between historical MEM simulations (1948-1967) and ssp585 MEM simulations (2068-2087) for IPSL-CM6-LR model.

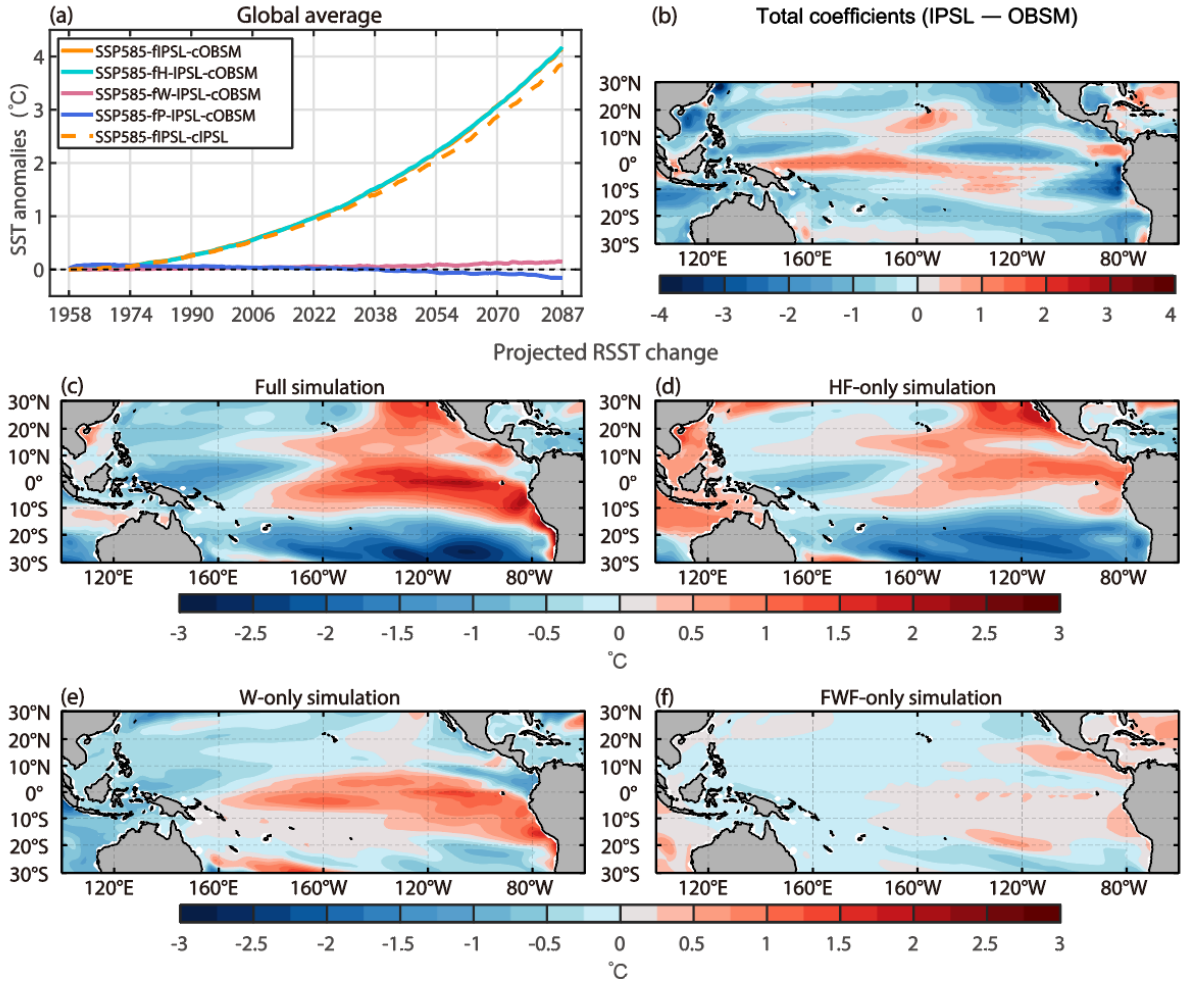

Figure 10: Process-oriented simulations. (a) Globally-averaged SST difference (°C) relative to CTL simulation for CC-ALL (?? curve), CC-Q (?? curve), CC-τ (?? curve), CC-F (?? curve) simulations. (b) Same as panel (a) but for RSST difference (°C) in the Niño3 region. Tropical Pacific maps of RSST difference relative to CTL simulation for (c) CC, (d) CC-Q, (e) CC-S and (f) CC-F simulations over the 2068-2087 period.

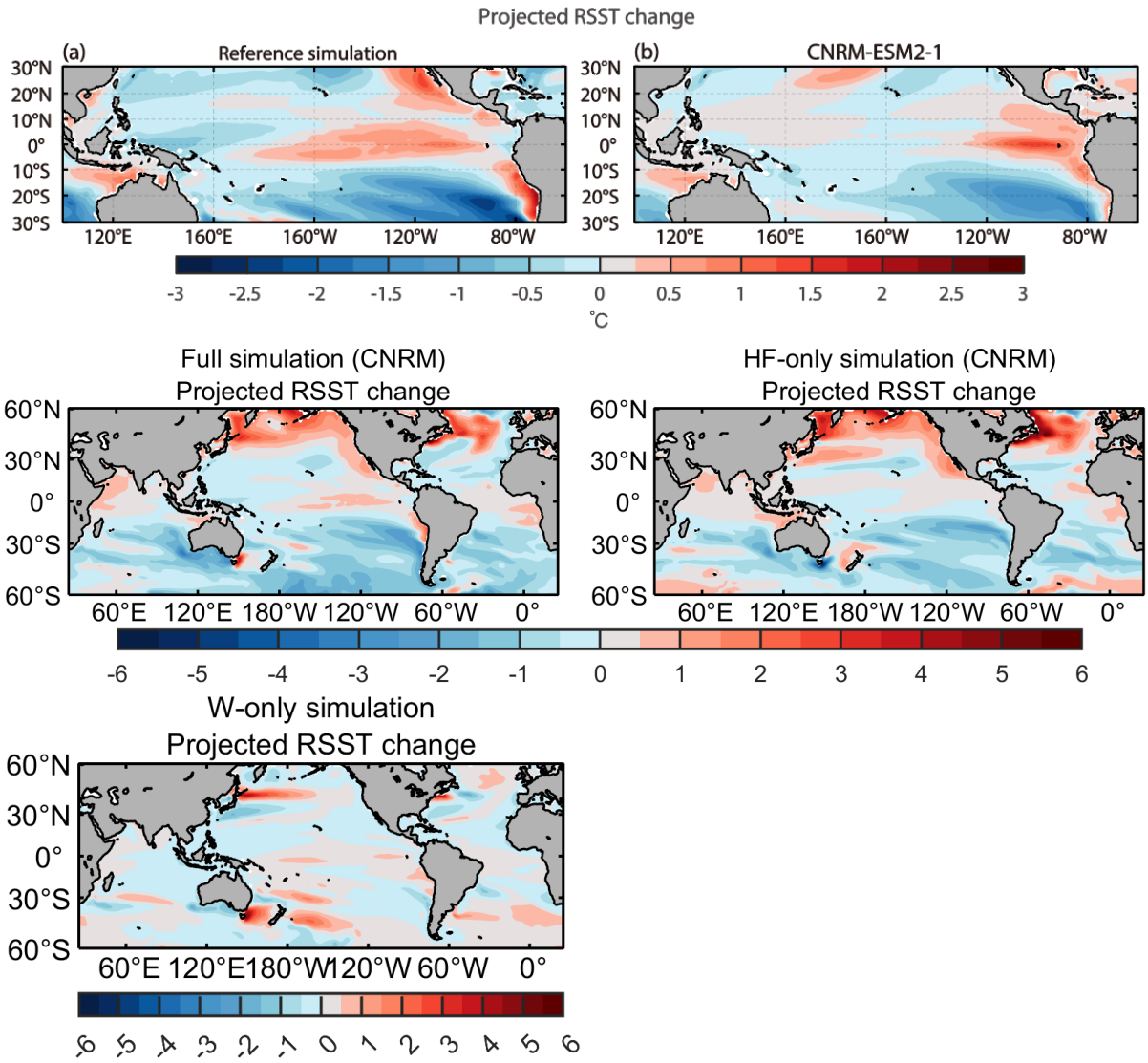

Figure 11: Application to the CNRM-ESM2-1 perturbations. Tropical Pacific maps of RSST (top; °C) difference for (a) CC-ALL, (c) CC-Q, (d) CC-Tau and (e) CC-F relative to CTL (2068-2087) and (b) between historical MEM simulations (1948-1967) and ssp585 MEM simulations (2068-2087) for CNRM-ESM2-1 model.

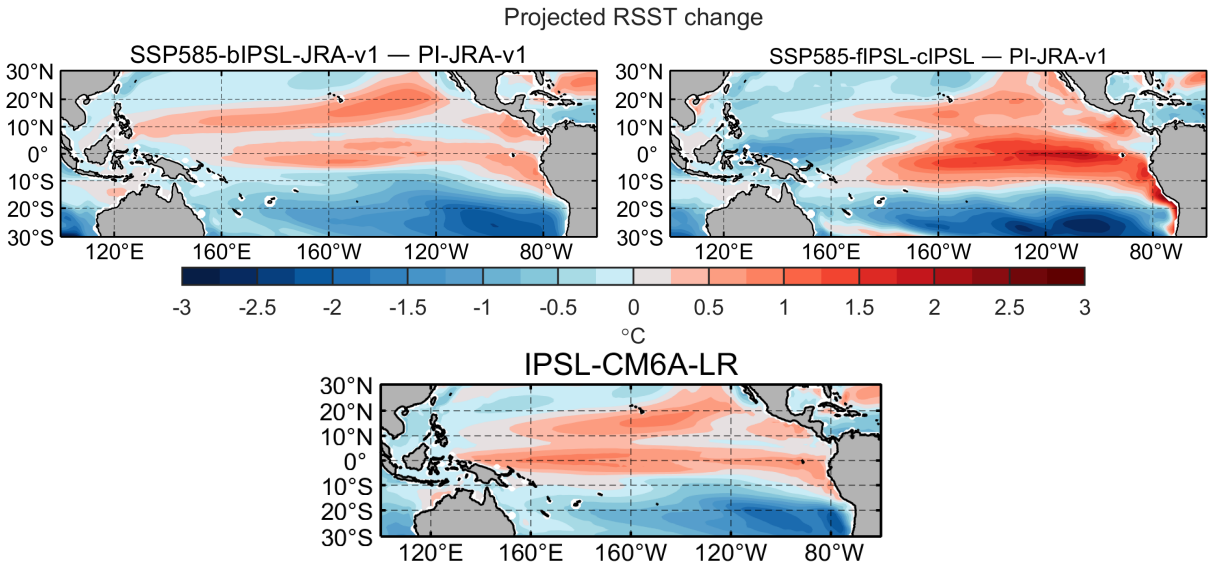

Figure 11: Bulk vs Flux-forced future simulations. (a) Globally-averaged SST difference (°C) for CC-ALL (?? curve) and CC-BULK (?? curve) relative to their corresponding control(CTL and bCTL) simulations. Tropical Pacific maps of RSST difference (°C) between (b) CC-BULK and CTL-BULK (2068-2087), between (c) CC-ALL and CTL (2068-2087), between (d) the IPSL-CM6A-LR SSP585 (2068-2087) and HIST (1948-1967) MEM simulation.